DOI:10.14753/SE.2022.2728

The functional importance of the intra-tumoral heterogeneity for extracellular vesicle release and uptake in colorectal cancer

Ph.D. thesis

Andrea Kelemen

Molecular Medicine Doctoral School

Semmelweis University

Supervisor: Zoltán Wiener, Ph.D., associate professor

Opponents: Ágnes Enyedi, Ph.D., senior research fellow
Krisztina Vellainé Takács, Ph.D., associate professor

Head of the Complex Examination Committee: Dóra Szabó, MD, D.Sc, professor

Members of the Complex Examination Committee: Mónika Lippai, Ph.D., senior lecturer
Balázs Mayer, Ph.D., senior research fellow

Budapest

2022

DOI:10.14753/SE.2022.2728

Table of content

Abbreviations 3
1. Introduction 7
1.1. Colorectal cancer 7
1.1.1 Epidemiology 7
1.1.2 Tumorigenesis and molecular subtypes 7
1.2. The canonical Wnt/β-catenin pathway 11
1.3. Intratumoral heterogeneity 13
1.3.1. Cellular heterogeneity in general 13
1.3.2. CD44 14
1.3.3. CD133 14
1.3.4. PTK7 15
1.3.5. IFITM1 15
1.4. The organoid technology 16
1.5. The tumor microenvironment 17
1.5.1. Cancer-associated fibroblasts 17
1.5.2. Extracellular vesicles 19
2. Objectives 21
3. Results 22
3.1. CD44 expression intensity marks CRC cells with different EV release capacity 22
3.2. CD44^{high} and CD44^{low} CRC cell-derived EV miRNA cargos show only a modest difference 24
3.3. Dose-dependent effect of CD44^{high} and CD44^{low} CRC organoid-derived EVs on fibroblasts 27
3.4. Ifitm1 expression is increased after *Apc* mutation 30
3.5. CRC patient-derived organoids have a heterogeneous expression of IFITM1 32
3.6. The IFITM1^{high} CRC population contains more proliferating cells 33
3.7. IFITM1^{high} and IFITM1^{low} CRC cells do not differ in their intensity of EV release 35
3.8. IFITM1^{high} CRC cells take up less EVs 38
3.9. Fibroblast-derived EVs result in a marked increase in the proliferating cell number of IFITM1^{low} CRC organoids 42
3.10. Deleting IFITM1 results in a higher EV uptake in CRC organoid cells 43

DOI:10.14753/SE.2022.2728

4. Discussion 45
5. Conclusions 50
6. Summary 51
7. References 52
8. Bibliography of the candidate's publications 66
9. Acknowledgments 68
10. Statement of originality 70

Abbreviations

APC: Adenomatous Polyposis Coli

ARF: Alternative Reading Frame

ASC: Adult Stem Cells

ATM: Ataxia-Telangiectasia Mutated

ATP: Adenosine triphosphate

CAF: Cancer Associated Fibroblast

CAV1: Caveolin 1

CCK4: Colon Carcinoma Kinase 4

CDH2: Cadherin-2

CDKN1A: Cyclin-dependent kinase inhibitor 1

CIMP: CpG Island Methylator Phenotype

CIN: Chromosomal Instability

CRC: Colorectal Cancer

DVL: Dishevelled

ECM: Extracellular Matrix

EGF: Epidermal Growth Factor

EGFR: Epidermal Growth Factor Receptor

EHS: Engelbreth-Holm-Swarm mouse sarcoma

EMT: Epithelial-Mesenchymal Transition

ENC1: Ectoderm-Neural Cortex Protein 1

EV: Extracellular Vesicle

FAP: Fibroblast Activation Protein

GAS6: Growth Arrest Specific 6

GTP: Guanosine 5′-triphosphate

GTPase: Guanosine 5′-triphosphatase

HCV: Hepatitis C Virus

HER2: Human Epidermal Growth Factor Receptor 2

HGF: Hepatocyte Growth Factor

HNF4A: Hepatocyte Nuclear Factor 4 Alpha

IFITM: Interferon-Induced Transmembrane Protein

IGF2: Insulin-Like Growth Factor 2

IL-1: Interleukin-1

IL-6: Interleukin-6

ITH: Intratumoral Heterogeneity

KRAS: Kirsten Rat Sarcoma Viral Oncogene

lEV: Large extracellular vesicle

MDM2: Mouse Double Minute 2 Homologue Protein

miRNA: microribonucleic acid

mEV: Medium extracellular vesicle

MLH1: MutL Homologue 1

MMR: Mismatch Repair

MSH2: MutS Homologue 2

MSH6: MutS Homologue 6

MSH6: MutS Homologue 6

MSI: Microsatellite Instability

MSS: Microsatellite Stability

MV: Microvesicles

MVB: Multivesicular Body

NK cell: Natural Killer Cells

PDL1: Programmed Cell Death 1 Ligand 1

PIK3CA: Phosphatidylinositol-4,5-Bisphosphate 3-Kinase Catalytic Subunit Alpha

PMS2: PMS1 Homologue 2

PSC: Pluripotent stem cell

PTEN: Phosphatase and Tensin Homolog

PTK7: Inactive Tyrosine-Protein Kinase 7

PTM: post-translational modification

RNF6: Ring Finger Protein 6

ROS: Reactive Oxygen Species

RTK: Receptor Tyrosine Kinase

SEMA5A: Semaphorin-5A

sEV: Small extracellular vesicle

SLC7A2: Cationic Amino Acid Transporter 2

SMAD4: SMAD family 4

SRF: Serum Response Factor

ST6GALNAC5: Alpha-N-acetylgalactosaminide alpha-2,6-sialyltransferase 5

STR: Short Tandem Repeat

TCF/LEF: T cell-Specific Factor /Lymphoid Enhancer-Binding Factor

TGF β: Transforming Growth Factor-β

TGFB2: Transforming Growth Factor Beta-2 Proprotein

TGFBR2: Transforming Growth Factor Beta Receptor 2

TME: Tumor Microenvironment

TNFSF4: Tumor Necrosis Factor Ligand Superfamily Member 4

TNFα: Tumor Necrosis Factor-Alpha

TP53: Tumor Protein 53 Gene

TSG101: Tumor Susceptibility Gene 101 Protein

VIM: Vimentin

YAP/TAZ: Yes1 Associated Transcriptional Regulator/Transcriptional Coactivator YAP1

αSMA: Alpha-Smooth Muscle Actin

DOI:10.14753/SE.2022.2728

1. Introduction

1.1. Colorectal cancer

1.1.1 Epidemiology

Colorectal cancer (CRC) is one of the most prevalent cancer types and the second leading cause of cancer death in developed countries. The incidence is associated with the level of socio-economic development of the region (*1*). CRC typically has no specific symptoms at the early stages. When the symptoms arise, CRC is already severe and in the advanced stage where it shows invasive and malignant phenotype, frequently already with metastases formation. The diagnosis at this stage correlates with a worse survival probability. The survival rate shows significant differences among the Western countries. Hungary is a leading country on the list of age-standardized incidence rates (*2*). Therefore, examining the molecular pathomechanism of this public health problem is a major issue.

1.1.2 Tumorigenesis and molecular subtypes

CRC is one of the first solid tumors that has been characterized molecularly. Different pathways have been identified in CRC tumorigenesis. The three well-described models are the chromosomal instability (CIN), microsatellite instability (MSI), and CpG island methylator phenotype (CIMP) pathways. The CIN model was described by Vogelstein and colleagues (*3*). This model includes a sequential series of events where the accumulation of the 'driver' mutations leads first to adenoma and then to carcinoma stages **(Fig. 1).**

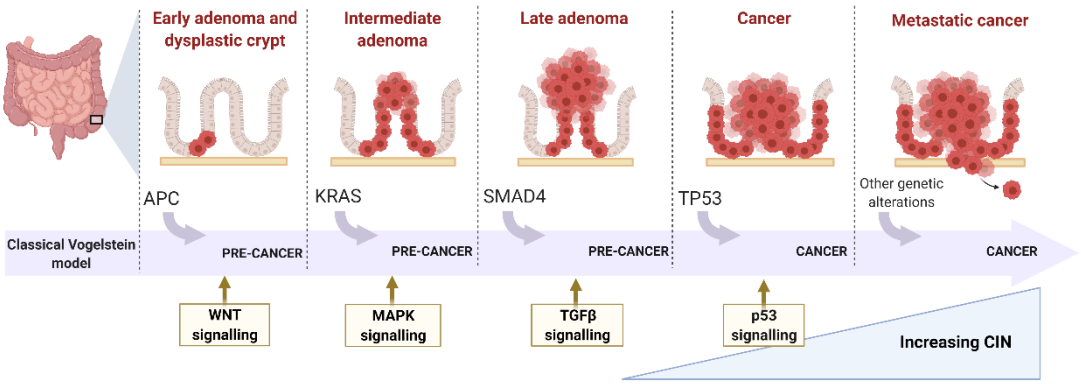

Figure 1: *The classical Vogelstein model. The order of the driver mutations and the affected pathways, meanwhile the chromosomal instability (CIN) increases.*

According to the Vogelstein model, the first and the most common driver mutation in patients (over 80 % occurrence) is the inactivation of the adenomatous polyposis coli (*APC*) gene. This mutation in the *APC* gene leads to a constitutive active Wnt pathway which causes an uncontrolled proliferation (*4*).

KRAS (kirsten rat sarcoma viral oncogene) is a member of the RAS gene family with GTPase activity. When it binds to guanosine 5′-triphosphate (GTP), KRAS turns active and transduces the signals to the downstream elements of the RAS-RAF-MAPK signaling cascade. This signal (e.g. epidermal growth factor, EGF) regulates cell proliferation and differentiation (*5*). The most common mutations of *KRAS* are G12D, G12V, and G12C (*6*). These mutations lead to constitutive active KRAS which causes aberrant and uncontrolled cell growth and cell transformation, promotes cancer metastasis, and also increases resistance to chemotherapy and EGFR targeted therapy in many cancer types including CRC (*7*).

SMAD4 plays a critical role in the transforming growth factor-beta (TGF-β) signaling pathway. In the presence of TGF-β the transmembrane serine-threonine kinase receptor, TGFβR transduces the signal and phosphorylates, therefore activating the SMAD proteins (*8*). After the activation, the SMADs can enter the nucleus and regulate the transcription of characteristic target genes. Several studies showed that loss of function mutations of the *SMAD4* tumor suppressor gene may contribute to the progression of CRC. Although it has been described that the mutation of SMAD4 can not induce tumorigenesis on its own, it can promote tumor progression caused by other genes (*9*).

Tumor protein 53 gene (*TP53*) is the most commonly mutated tumor suppressor gene in human cancers and this protein is regarded as „the guardian of the genome" with diverse functions. Depending on the specific context, it can induce cell cycle arrest, apoptosis, or senescence in the presence of cellular stress, such as DNA damage, hypoxia, or oncogene activation (*10*). The level of p53 protein is generally low due to the degrading activity of mouse double minute 2 homologue protein (MDM2). DNA damage promotes the post-translational modifications (PTMs) of p53 and it can trigger p53 to arrest the cell cycle via p21, enhance the transcription of pro-apoptotic (e.g. Bax) while inhibiting anti-apoptotic (e.g. Bcl-2) genes (*11*). Interestingly, oncogenic stress activates the expression

of the Alternative Reading Frame (*ARF*) to inhibit MDM2. The balance of the p53-MDM2 axis is crucial to prevent tumorigenesis (*12*).

This sequential accumulation of mutations initiates CRC carcinogenesis by deregulating pathways that modulate cellular differentiation, proliferation, and apoptosis. Alterations in the WNT–β-catenin, transforming growth factor-β (TGFβ), EGFR, and downstream MAPK and PI3K signaling pathways are nearly ubiquitous events in CRC (*13*). The above mentioned mutations provide the independent growth of the tumor cells from microenvironments factors, thus, these mutations are central events for tumor progression (*14*). With this phenomenon, the tumor shows an invasive phenotype and is more likely to form metastasis. Aneuploidy and loss of heterozygosity are present in 85 % of invasive CRC tumors (*15*). CIN arises from defects in chromosomal segregation, telomere stability, DNA damage response, and mutations in TP53 and other cell cycle checkpoint genes have a permissive role (*16*).

Microsatellites (MS), also called short tandem repeats (STR), are 1-6 nucleotide long repeats in the genome (*17*). Microsatellite instability (MSI) is caused by the mutation or silencing of the DNA mismatch repair system (MMR). The genetic or epigenetic alterations in the DNA repair genes mutL homologue 1 (*MLH1*), mutS homologue 2 (*MSH2*), mutS homologue 6 (*MSH6*), and PMS1 homologue 2 (*PMS2*) are found in 15% of CRC and this is characteristic for some sessile serrated adenomas (*18*). This dominant genomic feature results in hypermutation as well. Epigenetic studies showed that MSI correlates with the high CpG island methylation phenotype. The survival rate of patients with MSI is generally better than with microsatellite stability (MSS) and the chemotherapy is contraindicated (*19*).

On the transcriptomic level, CRC has recently been classified into four consensus molecular subtypes (CMS). The authors highlighted that although the model needed more refinement in the near future, however, this is currently the best way to capture CRC heterogeneity at the gene expression level and it is based on an agreement among many research groups (*16*, *20*, *21*). The mechanism of tumorigenesis of the different CMS groups is not well defined, different colonic cell types with oncogenic mutations may result in these CRC pathogenesis pathways.

DOI:10.14753/SE.2022.2728

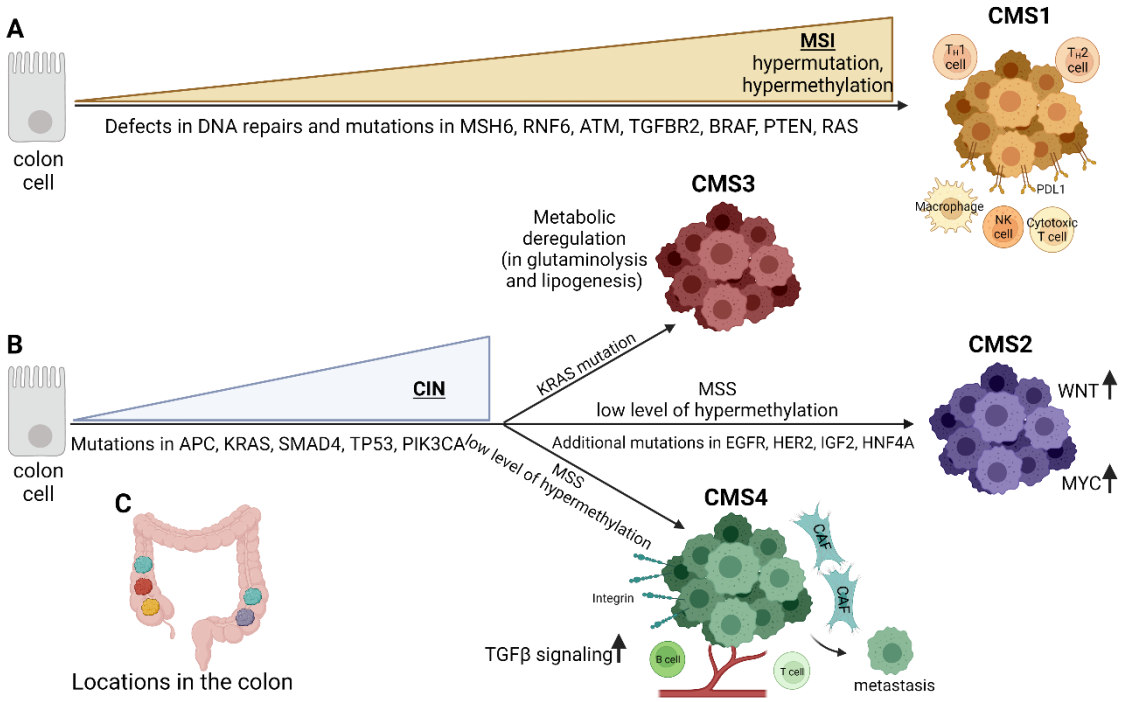

Figure 2: *The consensus molecular subtypes (CMS) of CRC and their characteristic localization in the colon.* ***A****: The characteristic features of the CMS1 subgroup* ***B****: The characteristic features of CMS2-4* ***C****:The localization of the four CMS subgroups, the different colours follow the A and B part of the figure and mark the different subtypes*

CMS1 (**Fig. 2A**) overlaps with the MSI cluster, thus, characterized by hypermutation and hypermethylation, and shows the massive infiltration of immune cells in the tumor microenvironment, such as CD8+ cytotoxic T lymphocytes, CD4+ T helper cells, and natural killer cells. In this type, the TGF-β signaling shows low activity and the majority of the cancer cells are Programmed cell death 1 ligand 1 (PDL1) positive. The defects of the DNA repair system is characteristic, moreover, mutations can frequently occur in the *BRAF* and *KRAS*, in MutS Homolog 6 (MSH6), Ring Finger Protein 43 (RNF43), Ataxia-Telangiectasia Mutated (ATM), Transforming Growth Factor Beta Receptor 2 (TGFBR2) and Phosphatase and Tensin homolog (PTEN) genes. The appearance of CMS1 tumors is the most common in the proximal colon (**Fig. 2C**) with solid, trabecular, or mucinosus features. Only 14 % of the tumors can be classified into this subtype and it has a good prognosis in early-stage tumors, although it has worse survival rates after relapse. CIN can be divided into three subgroups according to gene expression patterns (*22*).

CMS2 (**Fig. 2B**) is the canonical subtype that shows epithelial cell signature and a markedly high upregulation of WNT and the proto-oncogene MYC downstream targets. (*16*) MYC is partially under the control of the WNT pathway and it is a transcription

factor that regulates the transcription of several growth-related genes (*23*). Furthermore, this subtype shows microsatellite stability (MSS) and a low level of hypermethylation. Copy number gain mutations are more frequent in CMS2, leading to the overexpression of oncogenes such as Epidermal Growth Factor Receptor (EGFR), Human Epidermal Growth Factor Receptor 2 (HER2), Insulin-Like Growth Factor 2 (IGF2), Insulin receptor substrate 2 (IRS2) and Hepatocyte Nuclear Factor 4 Alpha (HNF4A). Moreover, the copy number losses in tumor suppressor genes are also characteristic. CMS2 marks mainly left-sided colon tumors (**Fig. 2C**) with complex tubular structures in the lower colon crypt compartments. The majority (37 %) of CRC patients have this subtype, it has superior survival rates after relapse with a larger proportion of long-term survivors (*22*).

CMS3 (**Fig. 2B**) is the metabolic subtype with the activation of glutaminolysis and lipogenesis and frequent *KRAS* mutations. It has a distinctive global genomic and epigenomic profile. However, hypermutation is present in this subtype, but the copy number alterations are not characteristic. The number of genes with hypermethylation is intermediate. The upper colon crypt compartments are involved and the tumors have a papillary morphology (**Fig. 2C**). Only 13% of the early-stage tumors are classified into this group (*24*).

CMS4 (**Fig. 2B**) is the mesenchymal subtype that is characterized by activation of epithelial-mesenchymal transition (EMT) pathways, tumor growth factor β (TGF β) signaling, integrin overexpression, and the accumulation of stromal fibroblasts. Due to the prominent stromal cell infiltration, the desmoplastic reaction is frequent (*24*). Immune cells are also important via e.g. complement signaling. This group shows MSS and only a low level of gene hypermethylation, similarly to CMS2. CMS4 shows the worst prognosis, due to the higher risk of distant relapse. About 23% of CRC patients can be classified into CMS4 (*16*). The characteristic localizations of the subtypes are shown in **Fig. 2C**.

1.2. The canonical Wnt/β-catenin pathway

The canonical Wnt pathway is one of the most prominent signaling pathways in CRC. It is a highly conserved axis that plays a significant role in tissue homeostasis, proliferation, apoptosis, differentiation, migration, and invasion. According to the literature, this pathway contributes not only to embryonic development but also to the tumorigenesis of

solid tumors and hematological malignancies (*24*). Without external Wnt ligands, the activity of a cytoplasmic destruction complex containing e.g. APC, AXIN, CK1, and GSK3β results in the phosphorylation and ultimately to the proteasomal degradation of β-catenin. In addition, critical transcription factors at the end of the Wnt pathway (TCF4, LEF1) are repressed and the Wnt pathway target genes are not expressed (**Fig. 3A**). In the presence of the secreted cysteine-rich glycoprotein ligands, the Wnt proteins, such as Wnt3a, the pathway is activated. The ligand binds to the complex of LRP-5/6 and the seven-transmembrane protein, Frizzled receptors. This cell surface signal induces Dishevelled (DVL) to recruit the members of the destruction complex to the receptor, leading to the inactivation of the complex. As a consequence, the degradation of β-catenin is inhibited, it accumulates in the cytoplasm and translocates into the nucleus where it functions as activating co-factor for transcription factors at the end of the Wnt pathway. This then results in the upregulation of T cell-specific factor (TCF)/lymphoid enhancer-binding factor (LEF) target genes, such as *c-Myc*, *cyclin D1*, Cyclin-dependent kinase inhibitor 1 (*CDKN1A*), *Axin2*, or *Lgr5* (*25*) (**Fig. 3B**). Interestingly, when R-Spondin proteins bind to Lgr5 on the cell surface, this ligand-receptor complex interacts with the LRP5/6-Frizzled-Wnt complex and inhibits its internalization and inactivation. Thus, the R-Spondin – Lgr5 complex extends the duration of Wnt signaling. Importantly, the Wnt pathway activity may be influenced not only by external Wnt signals but also by internal mutations. The mutation of members of the destruction complex leads to the unregulated and Wnt ligand-independent, constitutive activity of the pathway. The most frequent such mutation occurs in the *APC* gene in CRC patients (see above), leading to the inactivation of this protein (*26*) (**Fig. 3C**).

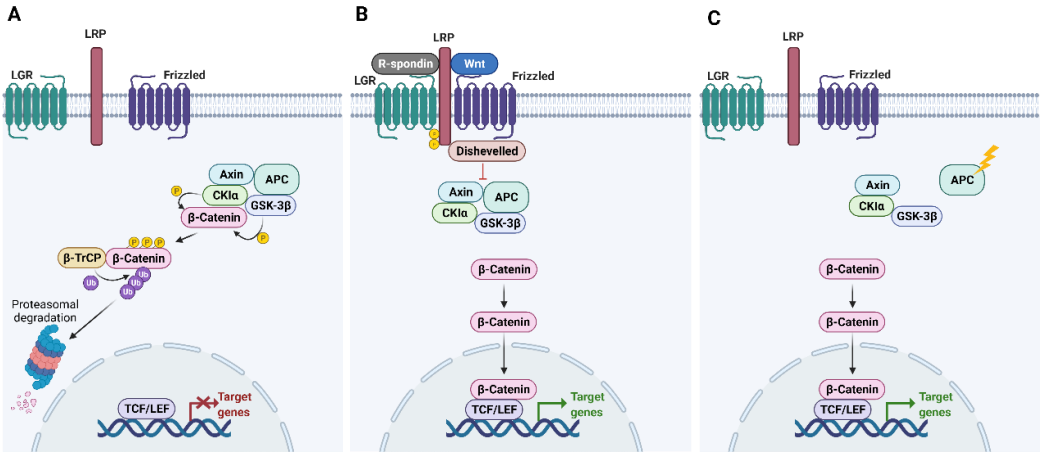

Figure 3:*The Wnt pathway* ***A****: The inactive Wnt pathway,* ***B****: The active Wnt pathway,* ***C****: The effect of APC mutation*

1.3. Intratumoral heterogeneity

1.3.1. Cellular heterogeneity in general

Tumor tissues are not an uniform mass of tumor cells, but they show a significant heterogeneity for both cancer and other cell types. Cancer heterogeneity can be observed both as inter- and intratumoral phenomenon. Inter-tumoral heterogeneity defines the variance among samples derived from the same histological type (*27*). Numerous patient-specific factors can contribute to inter-tumoral heterogeneity, such as genetic variations in the germline, the unique somatic mutation profile, and environmental factors. My dissertation focuses on intra-tumoral heterogeneity (ITH), meanwhile acknowledging the importance of inter-tumoral heterogeneity as well. ITH is characterized by spatial and temporal cellular diversity within a single patient sample that is a commonly overlooked hallmark of cancers. Tumors represent a cosmopolis for many cell types including cancer cells and stromal cells (e.g. fibroblasts, immune cells). Moreover, the majority of the tumors consist of genetically, epigenetically and as a consequence, phenotypically heterogeneous cancer cell subpopulations. ITH is the most challenging factor and often the most substantial roadblock in cancer treatment (*28*). The majority of tumors develop from a single or from a small group of mutated cells and they accumulate additional mutations as they progress to advanced disease (*29*). The driver mechanism is genomic instability which is critical in cancer development. This instability can derive from exogenous (e.g. UV radiation or tobacco smoke) and endogenous factors. The endogenous factor can be the aberrant operation of the DNA mismatch repairing (MMR) system. This malignant transformation leads to microsatellites instability (MSI) which causes an increased somatic mutation rate, not just at point mutation but also at the chromosomal level. Gains and losses of genome segments carry the possibility of segregation errors during cell divisions which promote the diversity by reformulating the activity of oncogenes and tumor suppressors. This mutational heterogeneity can result in forming more competitive subclones, a theory explained by the clonal evolution and selection hypothesis (*30*). The functions of these newly formed subpopulations have only in a few cases (e.g. LGR5, PROX1) been resolved so far (*31–33*). Although several mathematical models analyzed the ITH in CRC, none of them could calculate the effect of the tumor microenvironment on its phenotypic changes (*34*). Thus, CRC contains tumor cell populations with different molecular profiles. Understanding the critical role

of this intra-tumoral cellular heterogeneity in drug resistance, relapse and metastasis has just started to emerge. Thus, my dissertation focuses on the characterization of ITH with special interest in molecules that are connected to the Wnt pathway and that mark aggressive cell subpopulations.

1.3.2. CD44

CD44 is a glycoprotein with a single transmembrane domain, localized in the plasma membrane. The main ligand of this receptor is hyaluronic acid (HA). CD44 is encoded by 19 exons and due to the extensive alternative splicing, it has numerous isoforms. Ten exons take part in encoding the standard protein isoform. HA is a prominent component of the extracellular matrix (ECM). When HA binds to the extracellular ligand binding domain of CD44, the conformation changes of the cytoplasmic site triggers the activation of several signaling pathways. This event leads to cell proliferation, alteration in adhesion, migration, and invasion. CD44 is expressed on several cell types such as hematopoetic cells, embryonic stem cells, bone marrow cells, central nervous system, connective tissue, lung, and epidermis. A large collection of CD44 variants has been identified on epithelial cells. The expression of CD44 is upregulated in several types of cancers and it is a well described molecular marker for cancer stem-like cell subpopulations with aggressive features. This protein is overexpressed in cancer cells during epithelial-mesenchymal transition (EMT) (*35*, *36*). Transcription of CD44 is partially activated by Wnt signaling, and its overexpression is an early event in the transition from colorectal adenoma to carcinoma.

1.3.3. CD133

CD133, also called Prominin-1, is a five-transmembrane protein that is located in the plasmamembrane of protrusions and microvilli. This localization suggests that CD133 plays role in membrane organization. Some studies proposed the potential role of this protein in cellular fate decision and maintaining stem-like cell properties, although the exact molecular mechanisms remain elusive. CD133 is one of the first documented cancer stem-like cell markers in a wide array of tumor types. When isolated from primary colon cancer samples, CD133+ cells are capable of forming tumors in mice, remain undifferentiated in a serum-free medium and become more aggressive over the span of generations. CD133 expression therefore clearly characterizes CRC cell subpopulations with aggressive properties. In addition, CD133 plays an inductor role in the Wnt pathway

as the suppression of this protein has been described to inhibit the localization of β-catenin into the nucleus and the activation of the Wnt pathway (*37*).

1.3.4. PTK7

Inactive tyrosine-protein kinase 7 (PTK7), also called colon carcinoma kinase 4 (CCK4), is a member of the receptor protein tyrosine kinase (RTK) family. This plasma membrane protein is important in cell adhesion, cell migration, cell polarity, proliferation, actin cytoskeleton reorganization, and apoptosis. It has a catalytic role in phosphate transfer from adenosine triphosphate (ATP) onto tyrosine residues and is involved in the Wnt pathway (*38*). Several studies described that this protein is highly expressed in many cancer, in addition, PTK7+ CRC cells have a high Wnt and colony-forming activity in cell line models, suggesting that PTK7 marks an aggressive CRC cell population (*39*).

1.3.5. IFITM1

The human interferon-induced transmembrane (IFITM) protein family is encoded by five genes. Three out of the five IFITM proteins (IFITM1, IFITM2, and IFITM3) play a crucial role in virus uptake, thus, they critically contribute to cellular resistance against a wide range of membrane-surrounded viruses. IFITM5 and IFITM10 have no characterized roles in immunity. IFITM5 is required for normal bone mineralization, while the function of IFITM10 is unclear yet. Despite their names only the immune-related IFITM genes are interferon-inducible and even in the absence of interferon, they are expressed at a moderate to a high level in several tissues.

IFITM1 is localized in the plasma membrane and interacts with other transmembrane proteins, such as tetraspanins (e.g. CD81). The overexpression of IFITM1 has been described to inhibit the entry of Hepatitis C Virus (HCV) into the cells as well as the disruption of tight junction complexes. IFITM2 and IFITM3 have a similar effect on virus uptake, but they mostly reside in the endo-lysosomal compartment (*40*).

In a few studies, it has been reported that elevated IFITM1 expression correlates with worse outcomes and more aggressive phenotypes in CRC. Increased IFITM1 expression promoted, whereas decreased IFITM1 expression inhibited cell migration and tumorigenicity *in vitro*. In this process, the downstream target is the scaffold protein Caveolin-1 (CAV1), and over-expression of this molecule resulted in a more invasive phenotype (*41*).

1.4. The organoid technology

Organoids are three-dimensional (3D) *in vitro* growing structures derived from either PSCs (pluripotent stem cells) or ASCs (adult stem cells). They are self-organizing, assuming near-native microanatomy, with organ-specifically differentiated cell types and epithelial tissue arrangement (*42*). This technique allows the long-term maintenance of stem cell-based organotypic cultures. The organoid technology is a cutting-edge method to study the inter- and intratumoral heterogeneity. Due to differences between animal models and human cancers, patient-derived organoids are widely used to model the mechanisms of human tumorigenesis (*43*).

A further advantage of the technique is that cells do not have to adapt to two-dimensional (2D) growth as they grow in 3D under optimized and near-physiological conditions. Since only rare clones are able to survive and divide in 2D, cell lines undergo significant selection during cell culturing and they do not represent well the *in vivo* conditions. This problem does not arise in organoid technology, and samples from patients have been shown to be genetically stable. They are also suitable for genetic modifications (*44*). In addition, one of the advantages is that biobanks can be established from patient-derived organoids, thus, a large number of candidate molecules can be tested to discover novel effective drug combinations (*45*). Thus, in addition to basic research, this technology is also promising for clinical research (*46*). The organoid technology has emerged as a relatively low-cost and representative platform to model cancer heterogeneity and interactions with the tumor microenvironment *in vitro* (*47*).

In our experiments we used patient derived organoids. We dissociated the epithelium of the primary tumor and the normal colon by phisical and chemical procedures from surgical specimen and organoids were cultured in Mtarigel that is a widely used matrix in this technology. Normal colon organoids require the addition of several growth factors, among them the Wnt agonists Wnt3a and R-Spondin1. To select for cells with *APC* mutation and to exclude the survival or normal colon cells in tumor organoids, we cultured organoids without Wnt3a and R-Spondin1, thus, ensuring that only cells with a constitutively active Wnt pathway can survive. Importantly, organoid cultures contain only epithelial cells, but not mesenchymal cells (**Fig. 4**).

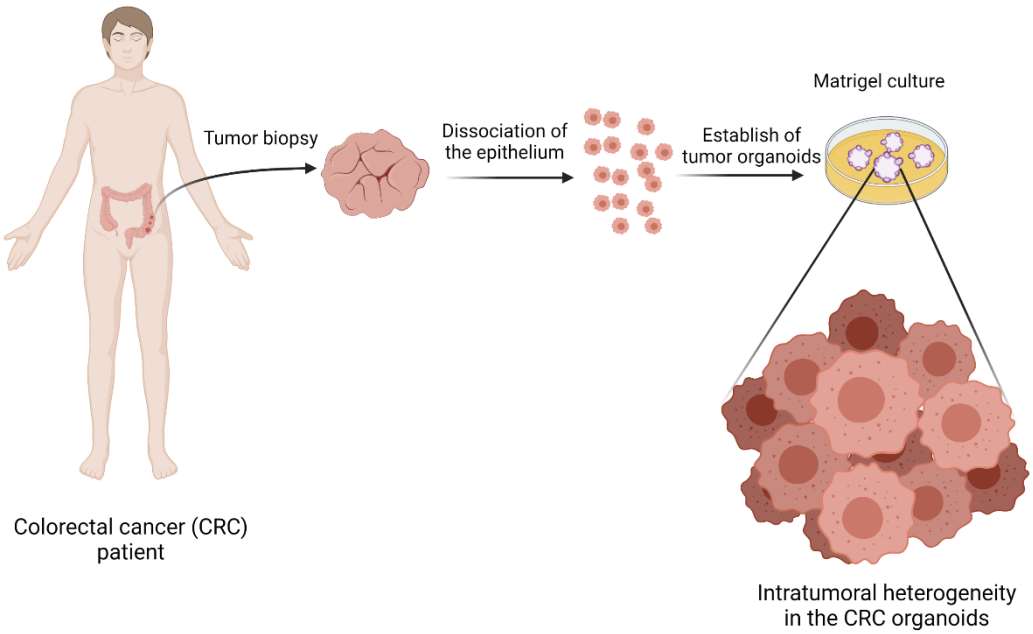

Figure 4: *The schematic figure of establishing organoid cultures*

Patient data for organoid lines (normal colon, adenoma or primary CRC) used in our studies are described in **Table1**. We used TNM classification system to define the stages of the tumor (T), the involvement of the lymph nodes (N) and the presence of metastasis (M).

Table 1 *Patient data for colorectal cancer, adenoma, and normal colon organoids. F: female, M: male*

No	Normal colon sample	Adenoma sample	CRC sample	Age	Sex	Diagnosis	TNM	Grade
1	-	-	+	63	F	adenocarcinoma	T3N0M0	2
2	-	-	+	74	M	adenocarcinoma	T3N0M0	2
3	-	-	+	75	M	adenocarcinoma	T3N2aM0	2
4	-	-	+	64	M	adenocarcinoma	T3N1bM0	1
5	+	-	-	56	M	adenocarcinoma	yT2N0	1
6	+	-	-	76	F	adenocarcinoma	T2N1a	1
7	+	+	-	67	F	colon adenoma	----	-
8	-	+	-	55	F	colon adenoma	----	-

1.5. The tumor microenvironment

1.5.1. Cancer-associated fibroblasts

Cancer-associated fibroblasts (CAFs) are a group of activated fibroblasts of mesenchymal origin. They secrete a variety of active molecules such as growth factors to alter the tumor microniche. Thus, they play a critical role in the generation and maintenance of the aggressive feature of some cancer cell subpopulations, immune regulation, angiogenesis,

metabolic response, extracellular matrix (ECM) remodeling, therapeutic resistance, and other biological processes. CAFs are present in the tumor tissue samples generally with an elongated spindle morphology. They are negative for non-mesenchymal (epithelial, endothelial, and leukocyte) biomarkers and positive for mesenchymal markers such as vimentin (VIM), alpha-smooth muscle actin (αSMA), fibroblast activation protein (FAP), and platelet-derived growth factor-alpha (PDGFα). Importantly, they usually do not carry important genetic mutations in cancers of epithelial origin (*48*). One prominent hallmark of some CRC subtypes is the accumulation and activation of fibroblasts. Furthermore, a strong negative correlation has been described between the amount of CAFs and the time to disease relapse in CRC. Fibroblast activation is associated with an increased expression of a characteristic group of genes including cadherin-2 (*CDH2),* ectoderm-neural cortex protein 1 (*ENC1*), tumor necrosis factor ligand superfamily member 4 (*TNFSF4*), alpha-N-acetylgalactosaminide alpha-2,6-sialyltransferase 5 (*ST6GALNAC5*), semaphorin-5A *(SEMA5A),* cationic amino acid transporter 2 (*SLC7A2*), and transforming growth factor beta-2 proprotein (*TGFB2*) (*60*). Activation of CAFs is driven by different pathways. TGFβ family ligands and lysophosphatidic acid activate fibroblasts via SMAD transcription factors and serum response factor (SRF), which leads to increased αSMA expression and the rearrangement of the cytoskeletal system. The physical contact between fibroblast and cancer cells can also promote their activation through Notch signaling in breast cancer (*49*). Various inflammatory signals such as interleukin-1 (IL-1), interleukin-6 (IL-6), and tumor necrosis factor-alpha (TNFα) can induce the CAF phenotype. Stress factors such as DNA damage, reactive oxygen species (ROS), or decomposition of the extracellular matrix, resulting in changes in its stiffness can also activate the fibroblasts.

The function of CAFs is also diverse. By remodeling the extracellular matrix and secreting soluble factors, such as hepatocyte growth factor (HGF) and growth arrest specific 6 (GAS6) factors they play a role in tumor cell invasion, thus, promoting metastasis formation. Additionally, they contribute to the crosstalk between macrophages, other immune cells, endothelial cells, and cancer cells by producing extracellular vesicles (*50*).

1.5.2. Extracellular vesicles

Extracellular vesicles (EVs) are membrane-surrounded structures released by virtually all cell types and they play a critical role in intercellular communication. Based on their biogenesis EVs can be classified into three main groups: exosomes, microvesicles, and apoptotic bodies. While exosomes are derived from the multivesicular bodies (MVBs) of the endosomal-lysosomal compartment, microvesicles (MV) are shed from the plasma membrane, and apoptotic bodies released by dying cells are regarded as EVs as well (*51*) (**Fig. 5**). The isolation of EVs according to their cellular origin holds difficulties, they are therefore often characterized by their size when purified with differential centrifugation and ultracentrifugation. This means that whereas the large EV (lEV) fraction is obtained when centrifuging the samples at a low speed, for medium EVs (mEV) usually a higher centrifugation speed and longer time are required. Small EVs (sEV) are pelleted after ultracentrifugation.

EVs carry biologically important molecules such as proteins, lipids, or miRNAs (**Fig. 5**). The most characteristic EV markers are the tetraspanins (CD9, CD63, CD81) which are four-transmembrane proteins, and the tumor susceptibility gene 101 protein (TSG101), which is part of the ESCRT-I complex. ESCRT complexes are critical in several membrane-related processes. ESCRT-0 recruits ESCRT-I to the membrane which is going to engulf, therefore the members of ESCRT-0 are essential for MVB formation. ESCRT-I interacts with either ESCRT-0 or ESCRT-II complexes. These three protein complexes play a role in the recognition of the ubiquitinated cargo. ESCRT-II initiates the assembly of ESCRT-III. These four ESCRT complexes together de-ubiquitinate the cargo and then ESCRT-III promotes the engulfment of the vesicle (*52*). Thus, CD9, CD63, CD81, and TSG101 markers play a significant role in EV biogenesis (*53*).

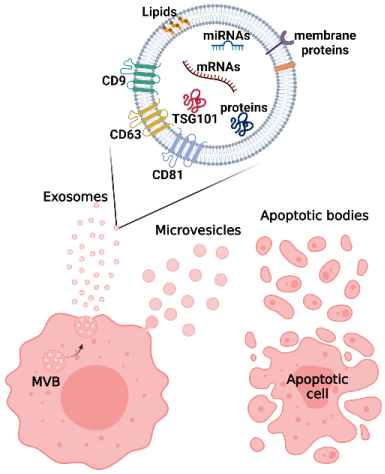

Figure 5: *The types of EVs based on their biogenesis, and the molecular cargo of EVs*

The role of EVs has been reported in several important procedures which is related to the tumor-stroma communication. EVs can induce the activation of the fibroblast and contribute to CAF formation. They are also important in establishing an invasive phenotype of the tumor cells and in invadopodia formation which is an invasive structure of the cells. Furthermore, tumor EVs take part in ECM remodelling by carrying matrix metalloproteases. CAF-derived EVs can induce the invasiveness of tumor cells by inducing the planar cell polarity pathway. Tumor EVs can also help to induce an increased vascular permeability and to form the metastatic niche in the recipient organs *(57)*.

In our all experiments, we followed the MISEV 2018 guideline for EV isolation and characterization (*54*). Since EVs transport their cargo in a protected way in the tissues and body fluids, and molecules specific for the releasing tumor cells are thought to be represented at a high concentration in EVs, they provide a promising tool for early cancer diagnostics. Furthermore, EVs can be edited and loaded with specific molecules, thus, they are rising weapons for targeted drug therapies as well (*55–57*).

DOI:10.14753/SE.2022.2728

2. Objectives

EVs are promising targets in early cancer diagnostics and since they can be loaded with different molecules, EVs may also hold a great promise for targeted therapy. However, whether all CRC cells can be targeted with a similar efficiency with EVs is not yet known. Thus, we aimed at identifying and characterizing the functional role of CRC cell subpopulations with differential EV uptake and release capacity. More specifically we set the following questions:

1. Are there subpopulations in CRC which release EVs at different level?
2. Do the subpopulation derived EVs have different EV miRNA cargo?
3. How do they contribute to fibroblast activation?

4. Which marker could characterize CRC cells with differential EV uptake?
5. Do these subpopulations have different proliferation potential?
6. What is the functional effect of the differential EV uptake in tumor organoids?
7. Does this molecule modify EV uptake or does it function only as a marker of CRC subpopulations?

DOI:10.14753/SE.2022.2728

3. Results

3.1. CD44 expression intensity marks CRC cells with different EV release capacity

Previously we proved that activating the Wnt pathway results in an elevation in EV release in an intestinal adenoma organoid model (*58*). To find molecules that may mark CRC cells with different EV release capacities, we focused on Wnt target cell surface molecules, which are also well described stem-like cell markers, thus, they mark CRC cell subpopulations with aggressive features. Therefore, we sorted patient-derived organoid cells based on their differential level of CD44, CD133, or PTK7. Importantly, by RT-qPCR and immunocytochemistry, we proved that the expression differences are maintained both at the mRNA and protein level even after 7 days in the 3D matrix. **(Fig. 6A-B)**

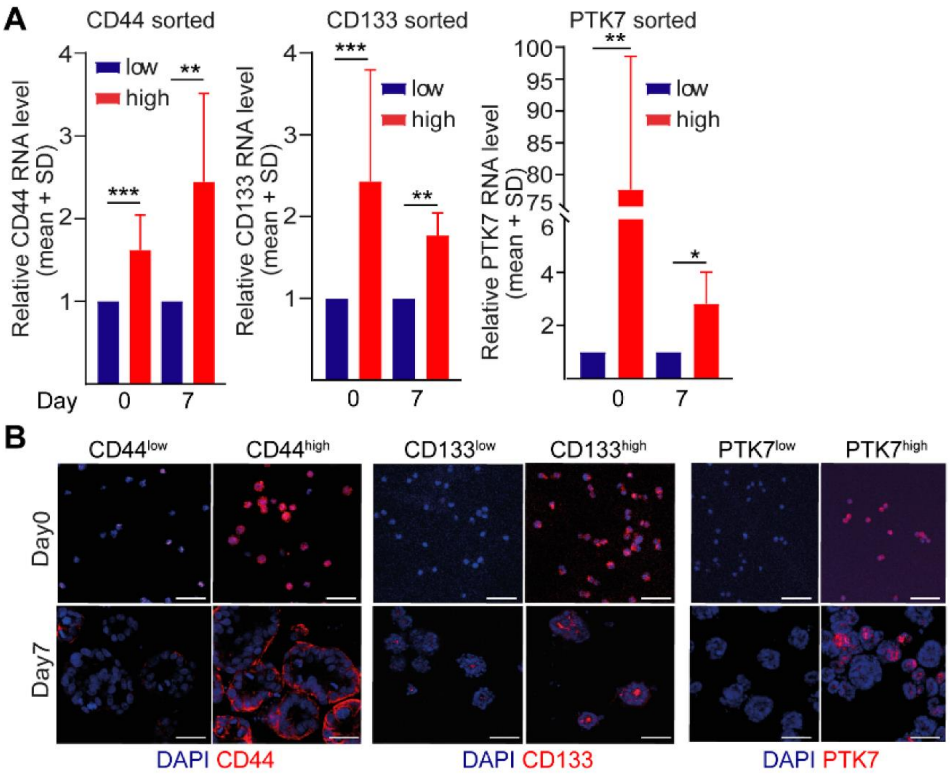

Figure 6*: The CD44, CD133, and PTK7 sorted cells maintain the expression difference even after 7 days.* ***A:*** *Relative RNA level after directly sorting (day 0) and 7 days after organoid formation. Data were normalized for the GAPDH housekeeping gene and the expression level in the CD44^{low}, CD133^{low,} and PTK7^{low} population was taken as 1 (RT–qPCR, n = 4 from four organoid lines). Statistical analysis: paired t-test, * p < 0.05, ** p < 0.01, and *** p < 0.005,* ***B:*** *Whole-mount immunostaining after directly sorting (day 0) and 7 days after organoid formation (confocal microscopic analysis, organoid #3)*

As the next step, we proved the presence of sEVs in CRC organoid-derived supernatants by antibody-coated beads that capture EVs and flow cytometry, by nanoparticle tracking analysis (NTA), transmission electron microscopy, and capillary-based immunoblot after ultracentrifugation (**Fig. 7A-D**).

Importantly, calnexin that is not associated with sEVs (*54*), was detected only in cell lysates, but not in sEV preparations. In contrast, the sEV marker TSG101 was present in the ultracentrifuged pellet. As a cellular control calnexin was used which is a resident protein in the endoplasmic reticulum. Notably, we detected calnexin only in the cell fraction and not in the the ultracentrifuged pellet. (**Fig. 7C**).

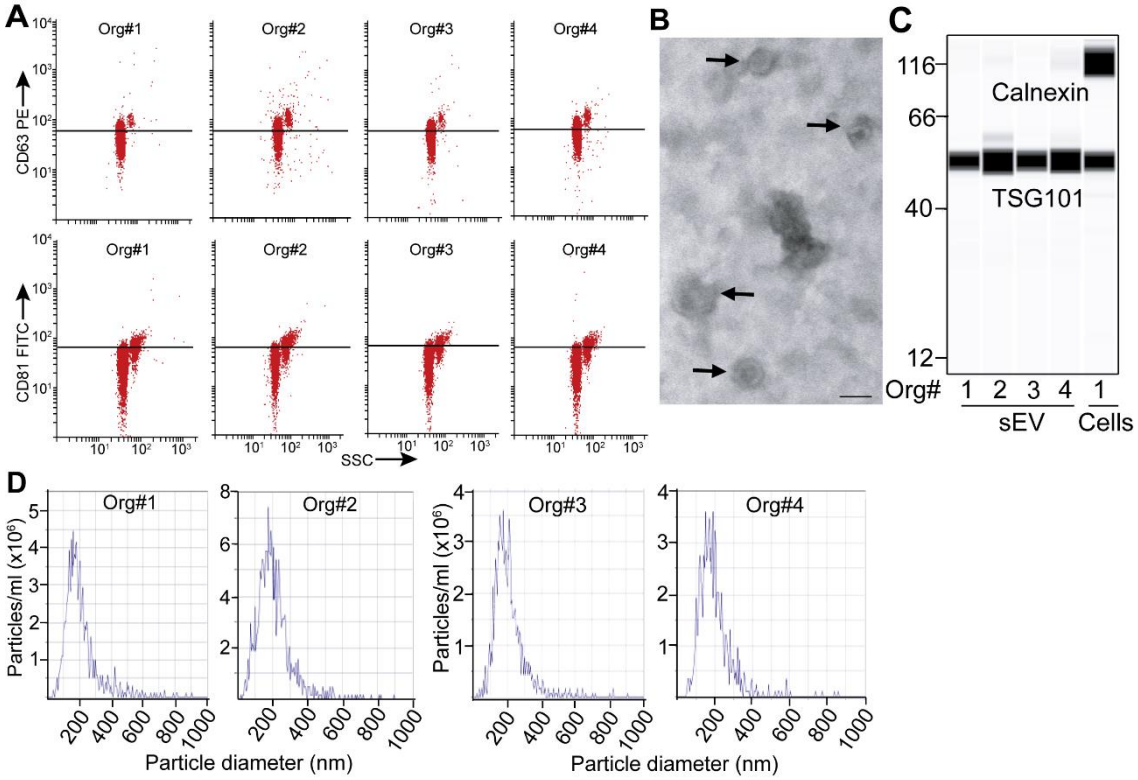

Figure 7: *Confirmation of the EV identity in the organoid conditioned media* ***A****: The CD63+ and CD81+ EVs were detected with the bead-based semiquantitative method. The samples were collected from organoid supernatants. The line marks the threshold from medium control.* ***B****: Transmission electron microscopic (TEM) image from an organoid supernatant after EV isolation by ultracentrifugation. Scale bar: 100 nm.* ***C****: Capillary-based WES immunoblot analysis of isolated sEV samples from four organoid lines. CRC cell lysates were used as control.* ***D****: The diameter distribution of sEVs among the four organoid lines by using nanoparticle tracking analysis (NTA)*

$CD44^{high}$ cell-derived organoids released more EVs compared to the $CD44^{low}$ subpopulation. We observed this difference in different 3D matrices (Matrigel that is rich at lamin and collagen IV, collagen I, and the mixture of them at 1:1 ratio). (**Fig. 8A**) In

contrast, we found no EV secretion difference in case of CD133 and PTK7 subpopulations, detected by NTA (**Fig. 8B-C**). We normalized the EV concentration for cell number, thus, our results did not reflect the different proliferation capacities of the cells. Collectively, our data suggest that high CD44 expression marks a CRC subpopulation with high EV release.

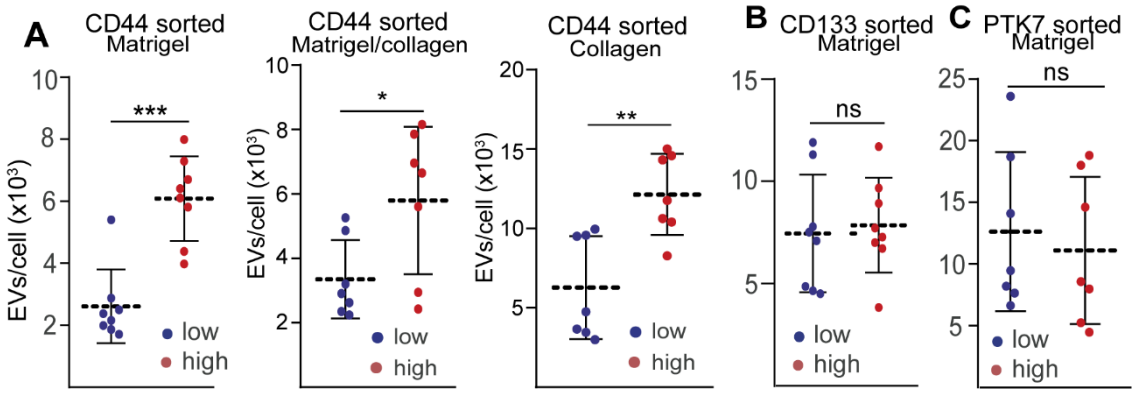

***Figure 8**: CD44^{high} cell-derived CRC organoids release more EVs than the CD44^{low} subpopulation. **A**: The released EV number per cell. The data are derived from the conditioned media of the organoids from sorted cells in Matrigel culture at day7. **B, C**: The released EV number per cell. The data are derived from the supernatants of the CD44 sorted organoid cells in Matrigel/collagen or collagen culture at day7. Statistical analysis: Mann–Whitney U test. * $p < 0.05$, ** $p < 0.01$, and *** $p < 0.005$*

3.2. CD44^{high} and CD44^{low} CRC cell-derived EV miRNA cargos show only a modest difference

As the next step, we compared the cargo of EVs from the different sorted subpopulations. Based on our previous data we used anti-CD63 and anti-CD81-coated beads to capture EVs from the supernatant of the organoids. This method provided us more pure EV samples with lower unspecific miRNA background compared to other methods (*59*). After the purification, we used Taqman low-density miRNA arrays. Our experimental setup is shown in **Fig. 9**.

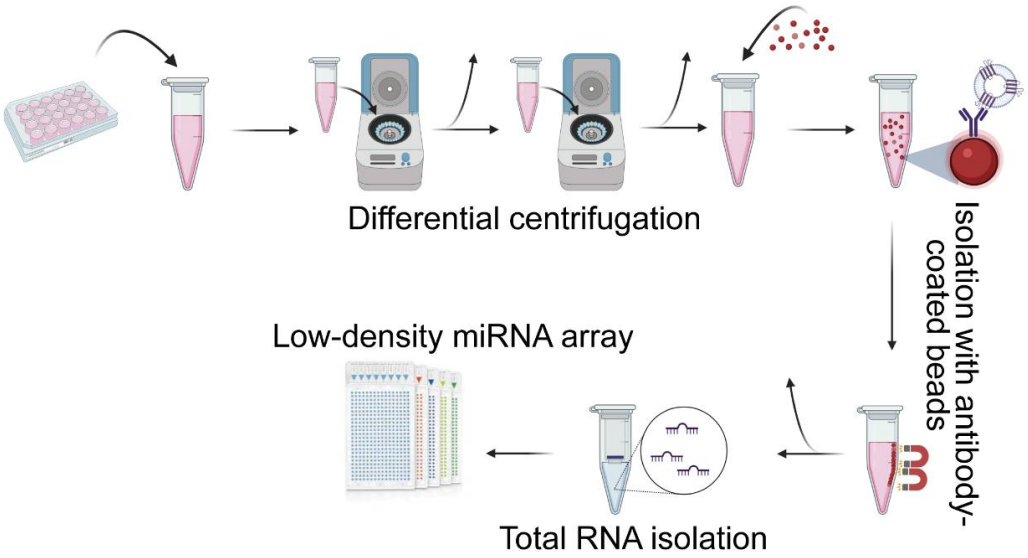

***Figure 9**: The experimental setup of EV isolation and miRNA cargo analysis*

As negative controls, we collected supernatants from cell-free Matrigel samples, the detected miRNAs were considered as background and they were excluded from further analysis. We focused only on miRNAs that were present in all biological parallels at least in one of the different subpopulations. We analyzed the presence and expression of 377 miRNAs, and we detected 26, 26, and 19 miRNAs when examining the overlap between organoids with different CD44, CD133, or PTK7 levels, respectively. We found only one miRNA differentially present in $CD133^{high}$ and $CD133^{low}$ organoid-derived EVs and no miRNAs were found to be specific for $PTK7^{high}$ or $PTK7^{low}$ CRC cell-derived EVs. Interestingly our analysis indicated that miR-95, miR-100, and miR-365 were specific for the $CD44^{high}$ and miR-345 for the $CD44^{low}$ organoid-derived EVs **(Fig. 10)**.

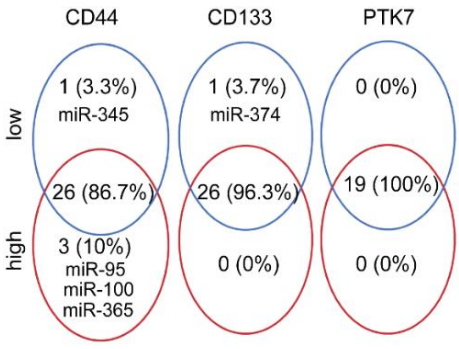

***Figure 10**: Venn diagram of the miRNA cargo of EVs derived from different sorted subpopulations. The number and the percentage of the miRNAs are represented.*

Since we found a significant overlap in the miRNA cargo between the respective subpopulations, we normalized EV cargo miRNAs to miR-19b levels since this miRNA

showed the most stable level among the samples. We used these normalized fold change values for linear discriminant analysis (LDA) to find miRNAs with differing levels between the experimental groups. When focusing only on miRNAs that were present in both the $CD44^{high}$ and the $CD44^{low}$ organoid-derived EVs, this bioinformatical method showed a higher level of miR-20a in $CD44^{low}$ cell-derived EVs as compared to EVs released by $CD44^{high}$ cells. Similarly, we found some differences in the levels of miR-27a, miR-92a, and miR-203 between EVs released by $CD133^{high}$ and $CD133^{low}$ organoids. However, EVs derived from different PTK7 subpopulations did not show any difference in their miRNA cargo patterns. **(Fig. 11)** Thus, we concluded that EVs released by CRC subpopulations had only a marginal difference in their miRNA cargo.

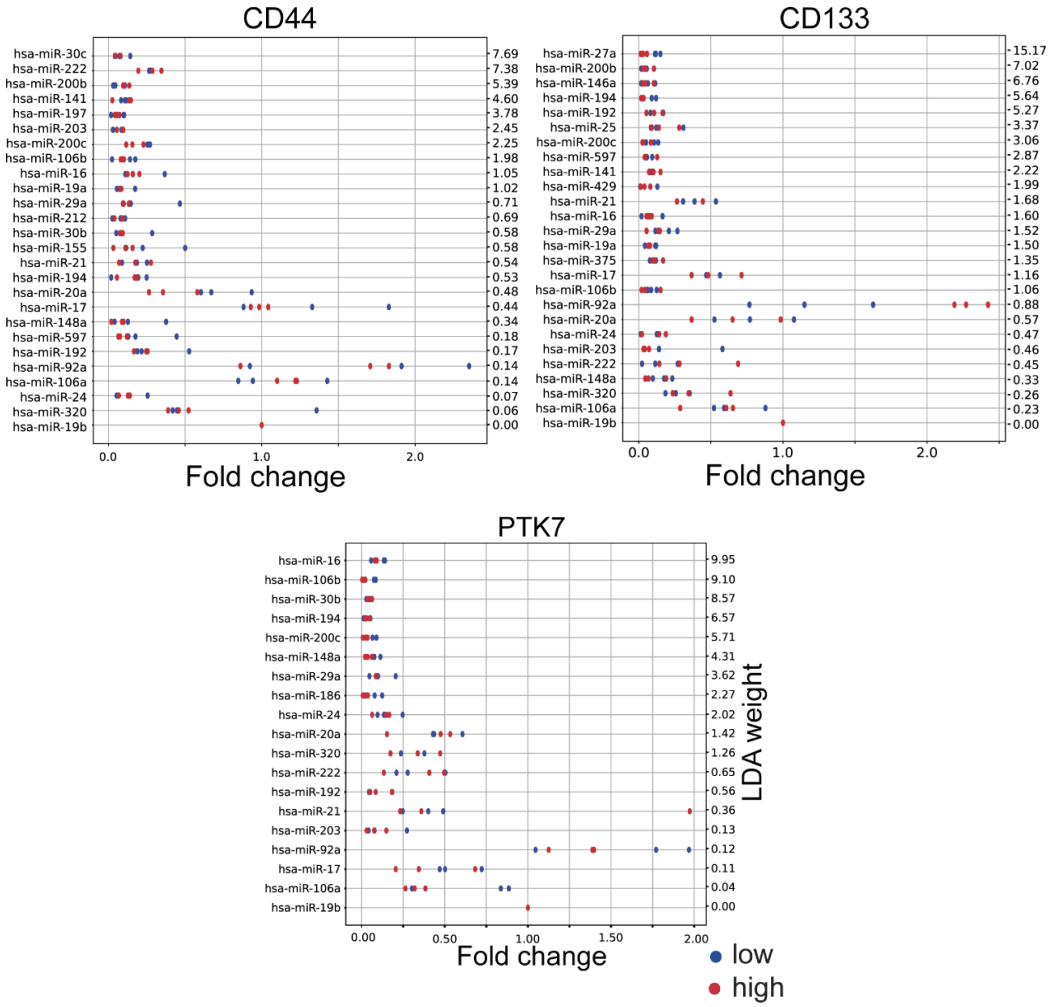

Figure 11: *Linear discriminant analysis (LDA) of the normalized levels of the overlapping miRNA cargo. For normalization miR-19b level was used. The normalized fold change values are marked as a dot in case of every detected miRNAs of the overlapping populations. The value of the LDA weight is higher if the two classes (high and low subpopulations) are more separated from each other based on the specific miRNA fold change. The bioinformatical analysis was performed by custom Python script.*

DOI:10.14753/SE.2022.2728

3.3. Dose-dependent effect of CD44^{high} and CD44^{low} CRC organoid-derived EVs on fibroblasts

To study the functionality of the differential miRNA cargo and secretion intensity of EVs from CD44^{high} and CD44^{low} CRC cells, we examined the effects of EVs on fibroblasts. Interestingly, when using EV amounts normalized to cell number, EVs secreted by CD44^{high} organoids induced a higher proportion of KI67+ proliferating colon fibroblasts compared to CD44^{low} cell-derived EVs. This proliferation capacity difference was not observed when testing EVs from identical numbers of CD133^{high} and CD133^{low} or PTK7^{high} and PTK7^{low} cells. (**Fig. 12A-D**).

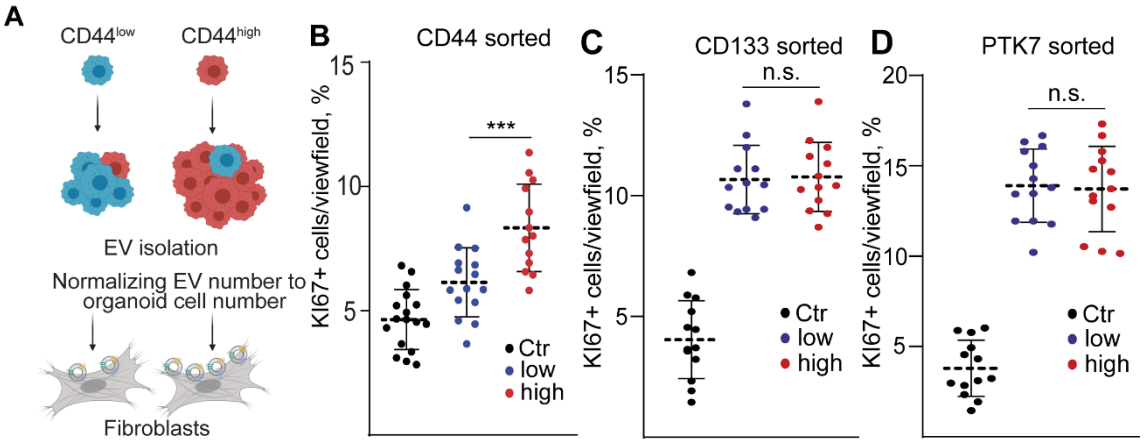

***Figure 12**: The effect of EVs isolated from different CRC cell subpopulations on fibroblast **A**: The schematic representation of the experimental workflow in the case of CD44 sorted CRC cells. EVs were derived from an identical number of cells. **B**: The percentage of KI67+ colon fibroblasts when applying EVs from 10^6 CD44 sorted cells at day 7. The treatment on the fibroblasts was carried out for 48h. Ctr: untreated control cells. The quantification was performed on confocal microscopic images. **C**: The percentage of KI67+ colon fibroblasts when applying EVs from 10^6 CD133 sorted cells at day 7. **D**: The percentage of KI67+ colon fibroblasts when applying EVs from 10^6 PTK7 sorted cells at day 7. Statistical analysis: Kruskal–Wallis and Dunn test, *** $p < 0.005$, n.s.>0.05*

To decide whether this effect was a purely dose-dependent phenomenon or based on the differential miRNA cargo, we repeated the experiments with an increasing amount of EVs isolated from CD44^{high} and CD44^{low} CRC cell subpopulations (**Fig 13A**). Of note, we observed that the percentage of KI67+ fibroblasts depended on the EV concentration, but it was independent of whether they had been isolated from CD44^{high} or CD44^{low} organoids. **(Fig 13B)**

DOI:10.14753/SE.2022.2728

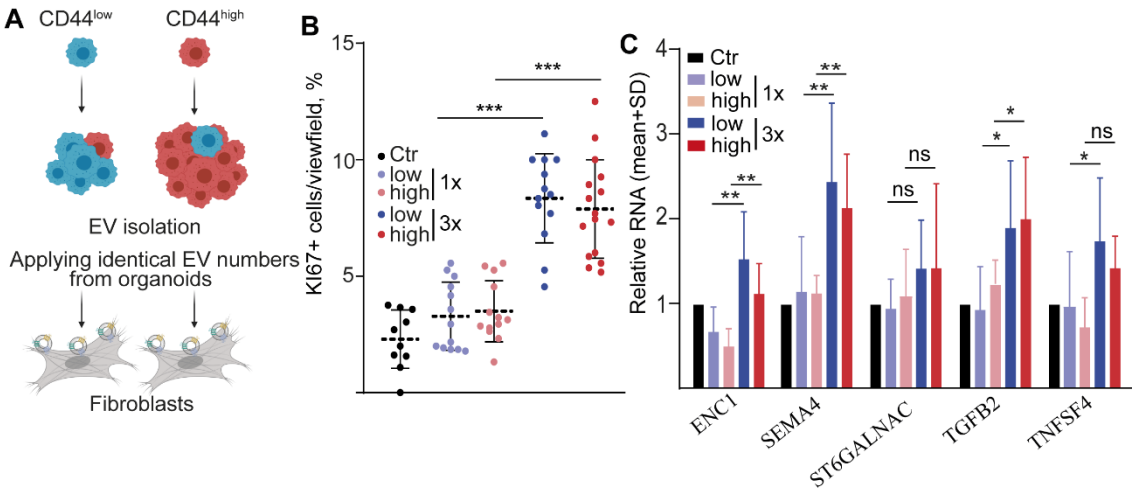

***Figure 13**: The effect of EVs on fibroblasts is dose-dependent **A**: The schematic representation of the experimental workflow. The fibroblasts were treated with identical numbers of EVs in different doses. **B**: The percentage of proliferating fibroblasts when applying increasing numbers of CD44^{high} or CD44^{low} organoid-derived EVs. The treatment on the fibroblast lasted for 48h. Ctr: cells without EV treatment. EV concentrations were 2 × 10^5/200 µL medium (1×) and 6 × 10^5/200 µL (3×). The quantification was performed on confocal microscopic images. Statistical analysis: Kruskal–Wallis and Dunn test, *** $p < 0.005$. **C**: RNA levels for the fibroblast activation marker genes in fibroblasts treated with CD44^{high} or CD44^{low} cell-derived EVs at increasing concentrations. EV concentrations were 2 × 10^5/200 µL medium (1×) and 6 × 10^5/200 µL (3×). Data were normalized to the GAPDH gene and then compared to the control (Ctr) samples that received no EVs. Of note, untreated control was taken as 1. (RT–qPCR, n = 4 from four organoid lines). Statistical analysis: paired t-test, * $p < 0.05$, and ** $p < 0.01$*

In addition, we stained the sorted cells with a membrane labeling dye. Fibroblasts were then treated with EVs isolated from conditioned media derived from the labeled organoids. We found no difference in the uptake intensity of CD44^{high} and CD44^{low} cell-derived EVs. Importantly, the concentration of the EVs was equal in this experiment (**Fig. 14A-B**).

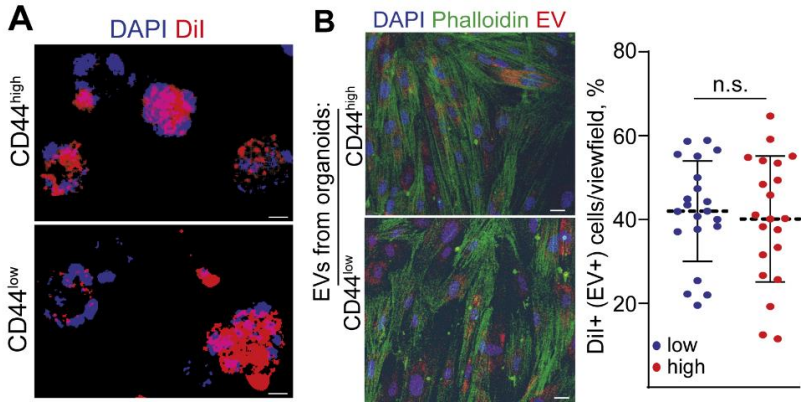

***Figure 14**:Fibroblasts take up EVs from CD44^{high} and CD44^{low} cell-derived organoids at a similar intensity **A:** CD44^{high} or CD44^{low} cell-derived organoids (org #2) labeled with the red fluorescent membrane dye DiI (representative confocal images.) Scale bars: 10µm **B:** Colon fibroblasts with fluorescent EV signal. EVs were collected from CD44^{high}*

or CD44^{low} cell-derived organoids (org #2) labeled with DiI and fibroblasts were treated with the labeled EVs for 24h. Representative confocal microscopic images (left panel) and their quantification. Note that untreated cells showed no red signal (not shown). Phalloidin was used to visualize cells. Statistical analysis: Mann-Whitney U-test, with n.s.>0.05. Scale bars: 10µm

These results indicate that it is not the differential miRNA cargo, but the number of EVs that is the critical factor. Furthermore, the expression level of activation markers in colon fibroblasts (*60*) depended on the number of EVs, and again, we could not find a difference between CD44^{low} and CD44^{high} cell-derived EVs. **(Fig. 13C)** Interestingly, the increasing amounts of liposomes that were artificially produced and contained no miRNA cargo had a similar, dose-dependent effect on both the proliferation rate and the expression level of activation markers in fibroblasts **(Fig. 15),** suggesting that the common miRNA cargo of CD44 subpopulation cell-derived EVs is not critical either. Collectively, these results indicate that: (i) fibroblast activation is induced by EVs or liposomes in a dose-dependent manner; (ii) the higher EV secretion by CD44^{high} CRC cells, and not the differential miRNA cargo is important in the differential effects of EVs derived from CD44^{high} and CD44^{low} cells.

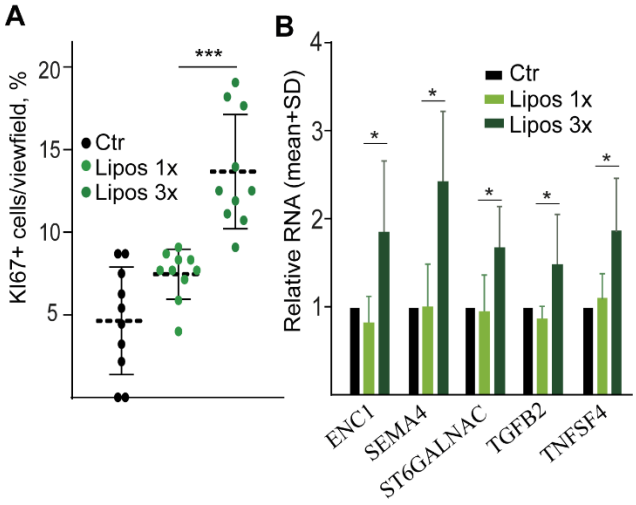

Figure 15: *Liposomes have the same dose-dependent effect as EVs from CD44^{high} and CD44^{low} cell derived organoid conditioned media.* ***A****: The percentage of KI67+ fibroblasts when applying increasing numbers of liposomes. Liposome concentrations were 2 × 10^5/200 µL medium (1×) and 6 × 10^5/200 µL (3×). The treatment on the fibroblasts lasted for 48h. Of note, untreated cells were used as control (Ctr). The quantification was performed on confocal microscopic images. Statistical analysis: Kruskal–Wallis and Dunn test, *** p < 0.005.* ***B****: Relative RNA levels of fibroblast activation marker genes when fibroblasts were treated with different amounts of liposomes. (RT–qPCR, n = 4 from independent experiments). Statistical analysis: paired t-test, * p < 0.05.*

3.4. Ifitm1 expression is increased after *Apc* mutation

As the next step, we aimed at identifying CRC cell subpopulations that take up EVs differently. Previously we had identified a set of genes that were activated by the loss of p53 and the activation of the Wnt pathway (the p53-suppressed invasiveness signature, PSIS) and which may account for the induction of invasiveness (*61*). To find genes that may be involved in the malignant behavior of CRC cells and EV uptake by CRC cells, we focused on IFITM1, a member of the PSIS gene set and the interferon-induced gene family with cell surface localization. Our bioinformatical data analysis (TCGA colorectal data sets, www.oncomine.org) showed that IFITM1 is highly overexpressed in CRC samples compared to normal colon and rectum (**Fig. 16A**), suggesting that IFITM1 is regulated by the Wnt pathway. To test this hypothesis, previously our research group established organoid cultures from wild-type (WT) mouse small intestine and introduced an *Apc* mutation to constantly activate the Wnt pathway. We performed gene expression analysis in these organoids. As expected, highly elevated RNA levels of the known Wnt targets *Lgr5*, *Axin2*, and *Myc* were observed (**Fig. 16B**). In addition, *Apc* mutation resulted in a pronounced increase in the expression of *Prox1*, an intestine-specific Wnt target gene (*62*), and, surprisingly, we detected a more than 2,500-fold increase in the expression of *Ifitm1* (**Fig. 16C**).

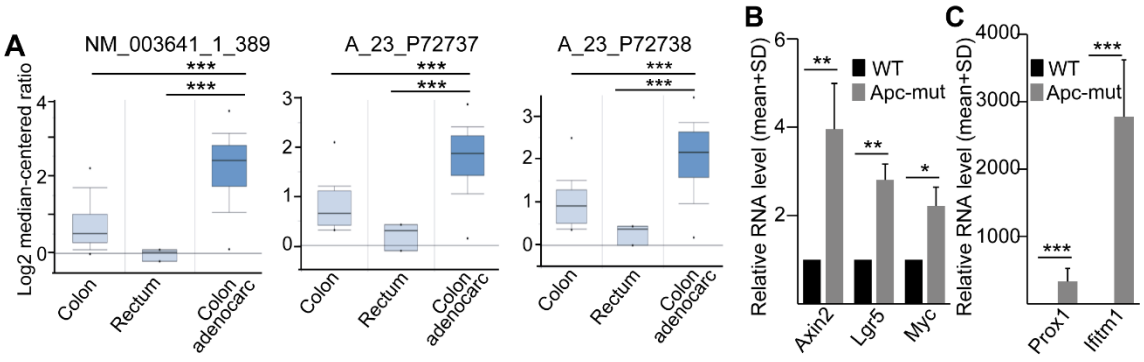

***Figure 16**: **A**: Bioinformatical analysis of the TCGA dataset in the Oncomine database (http://www.oncomine.org) for the indicated probes focusing on the IFITM1 expression level.). Statistical analysis: Unpaired t-test, *p < 0.05, **p < 0.01, ***p < 0.005, n.s.: p > 0.05 **B** Relative RNA levels of the indicated genes in wild type (WT) and Apc mutant mouse small intestinal organoids (RT-qPCR, n = 4). Statistical analysis: paired t-test, *p < 0.05, **p < 0.01, ***p < 0.005. **C** Relative RNA levels of Ifitm1 and the Wnt target gene Prox1 in the indicated mouse small intestinal organoids (RT-qPCR, n = 4), Statistical analysis: paired t-test, *p < 0.05, **p < 0.01, ***p < 0.005.*

To further study the regulation of IFITM1, we isolated organoids from the normal colonic (NCO) and the tumor (CRCO) samples of CRC patients. In addition, we collected samples from patients diagnosed with colon adenoma (AO) (see above patient data, **Table 1**).

AOs and CRCOs were cultured without the Wnt-agonist R-Spondin1 and Wnt3a, thus, samples were selected for organoids carrying *APC* mutation and harboring a constitutively active Wnt pathway. In our gene expression analysis, we detected higher RNA levels of not only *AXIN2*, *LGR5*, and *MYC*, but also of *IFITM1* in both AOs and CRCOs as compared to NCOs (**Fig. 17**).

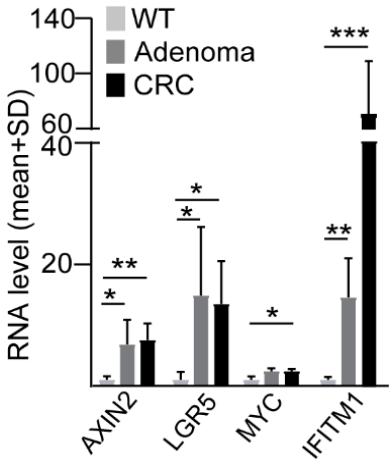

***Figure 17**: Wnt target genes and IFITM1 mRNA levels are significantly increased in adenoma and CRC organoids compared to normal colon (WT) organoids. Data were normalized to the GAPDH gene. WT was taken as 1. Statistical analysis: paired t-test. * $p < 0.05$, ** $p < 0.01$, and *** $p < 0.005$*

LGR5 marks a stem cell population in CRC and intestinal adenomas (*31*, *32*, *63*). To decide whether *Ifitm1* expression is specific for the Lgr5+ cells, we analyzed microarray data from sorted $Lgr5^{high}$ and $Lgr5^{low}$ mouse intestinal adenoma cells (*63*). Whereas the RNA levels of *Cd44* and *Cd133* were higher in the $Lgr5^{high}$ cell population, we found no difference in *Ifitm1* (**Fig. 18A**). Furthermore, whereas the RNA level of *CD133* was higher in $LGR5^{high}$ compared to $LGR5^{low}$ human CRC organoid cells in RNA expression datasets (*32*), we found no difference in *IFITM1* expression between the two cell populations (**Fig. 18B**). Collectively, these data suggested that *IFITM1* is under the regulation of the Wnt pathway, but it is not specific for the $LGR5^{high}$ CRC cells with stem cell features.

DOI:10.14753/SE.2022.2728

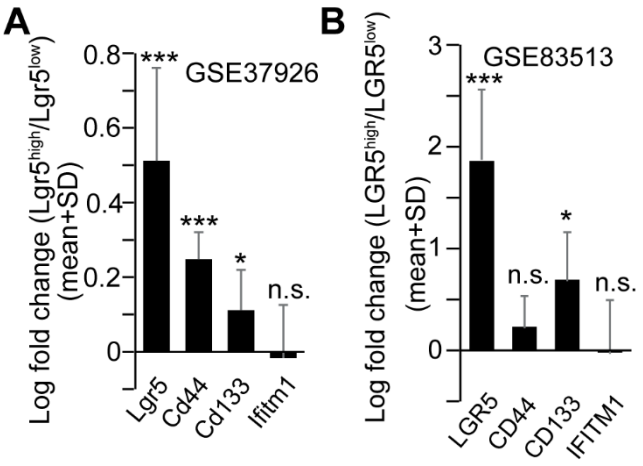

Figure 18: *IFITM1 is under the control of the Wnt pathway, however, its level does not correlate with LGR5 expression.* ***A****: Difference in the expression levels between Lgr5^{high} and Lgr5^{low} mouse adenoma cells for the indicated genes (bioinformatical analysis of the GSE83513 dataset with the GEO2R online tool). Statistical analysis: t-test with Benjamini and Hochberg false discovery rate, * p < 0.05, *** p < 0.005 and n.s.>0.05* ***B****: Comparing the expression levels of LGR5, CD44, CD133, and IFITM1 between LGR5^{high} and LGR5^{low} cells in CRC patient-derived organoids (GSE83513 dataset). Statistical analysis: t-test with Benjamini and Hochberg false discovery rate, * p < 0.05, *** p < 0.005 and n.s.>0.05*

3.5. CRC patient-derived organoids have a heterogeneous expression of IFITM1

Recent publications suggested that the C-terminal part of the IFITM1 protein faces the extracellular space (*64*, *65*). In line with these studies, we detected a flow cytometric signal with an antibody produced against the N-terminal part of IFITM1 only if cells had been permeabilized before labeling (**Fig. 19A-C**). In contrast, the antibody against the C-terminal part labeled cells without permeabilization as well (**Fig. 19B-C**). Interestingly, immunostaining showed the cellular heterogeneity in IFITM1 expression among organoids from the same patient (**Fig. 19D-E**). Furthermore, analysis of Protein Atlas data (www.proteinatlas.org) indicated that tumor cells of the same sample were heterogenous for the IFITM1 level (**Fig. 19F**). Thus, IFITM1 expression is heterogeneous among CRC cells within organoid lines.

DOI:10.14753/SE.2022.2728

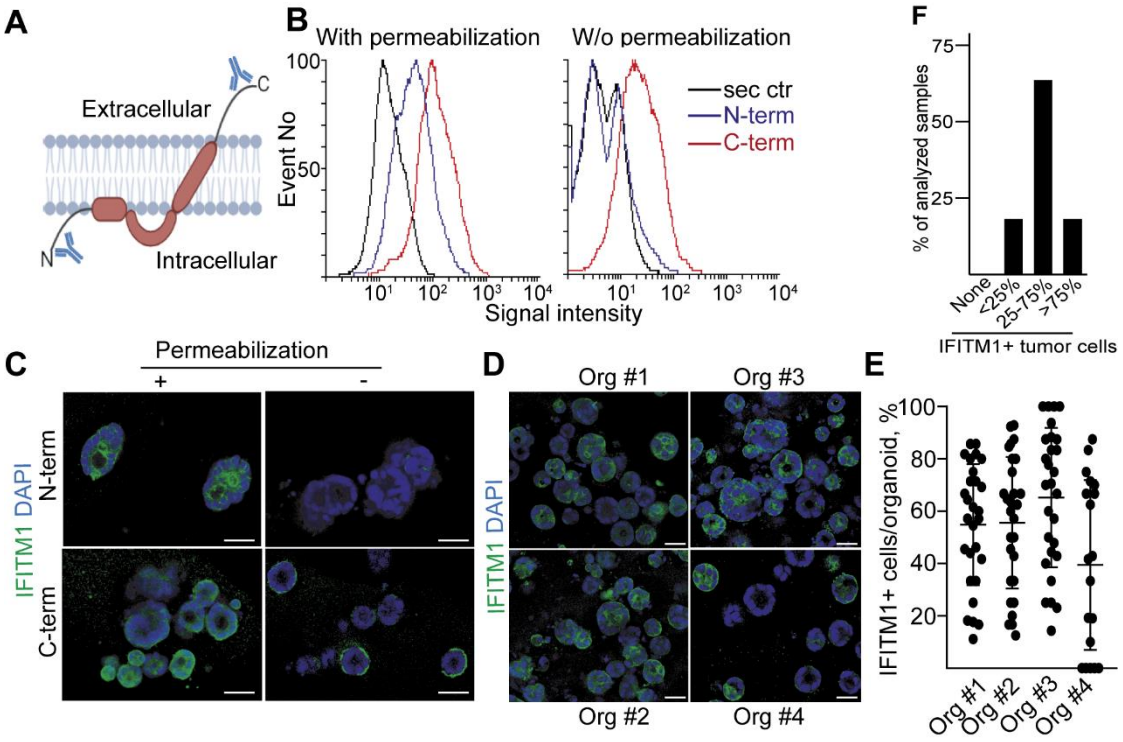

Figure 19 *The orientation of IFITM1 in the plasma membrane and its heterogeneity among the organoid lines* ***A****: Schematic representation of IFITM1 in the membrane showing the binding sites of the used antibodies.* ***B****: Flow cytometric analysis of the N- and C-terminal specific antibodies with and without cell membrane permeabilization. Notably, only the secondary antibody was used for control (sec ctr).* ***C****: Whole-mount immunocytochemistry with the N- and C-terminal specific antibodies with and without cell membrane permeabilization in CRC organoids. Scale bar: 50µm* ***D****: Whole-mount immunocytochemistry of the four organoid lines with the C-terminal antibody. Scale bar: 50µm* ***E****: The percentage of IFITM1+ cells among organoids. Quantification was performed on confocal microscopic images.* ***F****: The percentage of IFITM1+ cells among tissue samples. Analysis of the data from the online Protein Atlas, www.proteinatlas.org*

3.6. The IFITM1^{high} CRC population contains more proliferating cells

As the next step, we sorted CRC organoid cells based on their IFITM1 protein levels into IFITM1^{high} and IFITM1^{low} subpopulations. (**Fig. 20A**) Then we checked the efficiency of our sorting by flow cytometry and capillary-based immunoblotting (**Fig. 20A-B**) and used the samples for RNA analysis. Interestingly, no difference in the RNAs of the Wnt target genes *AXIN2*, *LGR5*, or *MYC* were observed, but IFITM1^{high} cells expressed the mesenchymal marker genes *VIM* and *ZEB1* at a lower level (**Fig. 20C**). Furthermore, we observed a decreased RNA expression of *CD133* (**Fig. 20C**). We counted the organoid forming units in the subpopulations, however, surprisingly, we detected no difference in the numbers of organoids. (**Fig. 20E**). Although the diameter of the organoids derived from IFITM1^{high} cells was significantly higher and they contained more KI67+

proliferating cells, there was no difference in the percentage of active caspase3+ apoptotic cells (**Fig. 20F-H**). Parallel with these findings, we observed lower RNA levels of the differentiation markers *MUC2* (Goblet cells) and *ALPI* (enterocytes) in IFITM1^{high} cell-derived organoids (**Fig. 20D**), showing the shift between proliferating and other cell types. Thus, although classical stem-like cell markers are not highly expressed in IFITM1^{high} cells, they produce organoids with a higher proliferation potential compared to the IFITM1^{low} subpopulation.

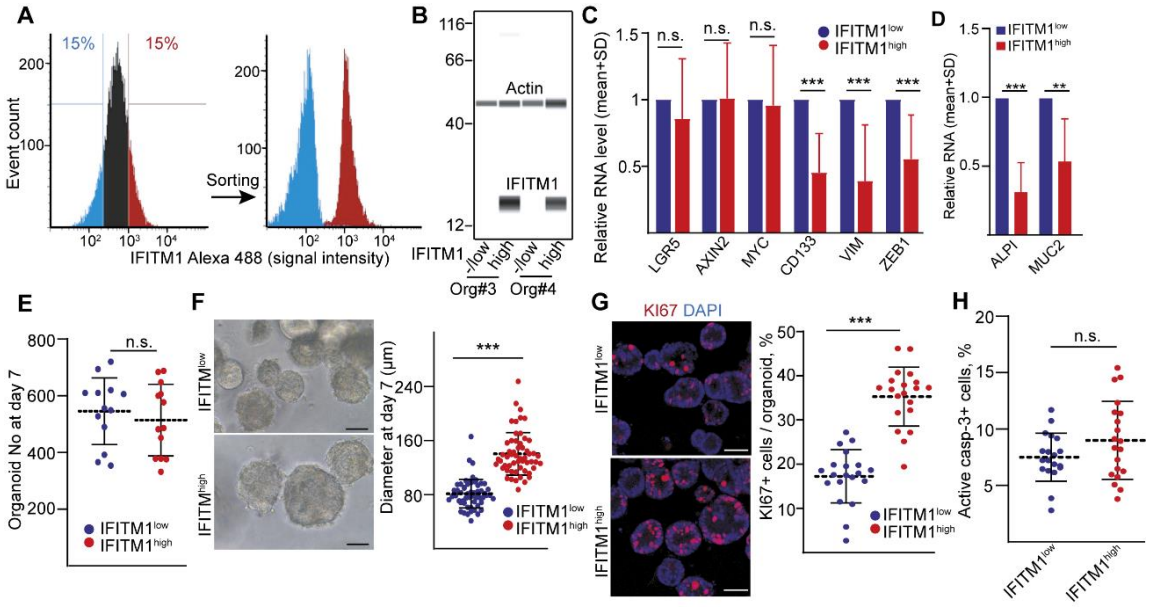

***Figure 20**: The IFITM1^{high} subpopulation contains more proliferating cells than IFITM1^{low} CRC cell-derived organoids **A**: The fluorescence sorting strategy for IFITM1 protein level and their repeated measurements after sorting. **B**: Capillary-based WES immunoblot analysis on the sorted cells at day0. **C**: Gene expression analysis of the IFITM1 sorted cells. Data were normalized to the GAPDH gene. IFITM^{low} subpopulation was taken as 1. Statistical analysis: paired t-test. *** $p < 0.005$ and n.s.>0.05 **D**: Gene expression analysis of the IFITM1 sorted cells. Data were normalized to the GAPDH gene. IFITM^{low} subpopulation was taken as 1. Statistical analysis: paired t-test. ** $p < 0.01$, and *** $p < 0.005$ **E**: The number of organoids initiated by 20,000 sorted cells at day 7. Each dot represents an individual sorting experiment. Statistical analysis: Mann–Whitney U-test, n.s. > 0.05 **F**: Representative brightfield photos of the sorted organoid at day 7(left) and the quantification of the organoid diameters (right). Scale bar: 50µm, statistical analysis: Mann–Whitney U-test, *** $p < 0.005$ **G**: Representative confocal images of the sorted organoids at day 7, whole-mount immunocytochemistry was performed for KI67 (left) and the quantification of the percentage of KI67+ cells in organoids (right). Scale bar: 50µm, statistical analysis: Mann–Whitney U-test, *** $p < 0.005$ **H**: The percentage of active caspase-3 positive cells in the organoids. Statistical analysis: Mann–Whitney U-test, n.s.>0.05*

DOI:10.14753/SE.2022.2728

3.7. IFITM1^{high} and IFITM1^{low} CRC cells do not differ in their intensity of EV release

The IFITM1 cell surface protein is involved in inhibiting the uptake of membrane-surrounded viruses (*66*, *67*), raising the possibility that this molecule regulates EV traffic as well. To study this hypothesis, we first set up an experimental method where we could culture the organoid cells in 2D conditions. We then measured the stability of IFITM1 expression compared to 3D cultures. Organoid-derived CRC cells were viable on Matrigel-coated plates (**Fig. 21A**) and we found no difference in cell surface IFITM1 expression between cells cultured either 2D or 3D (**Fig. 21B**).

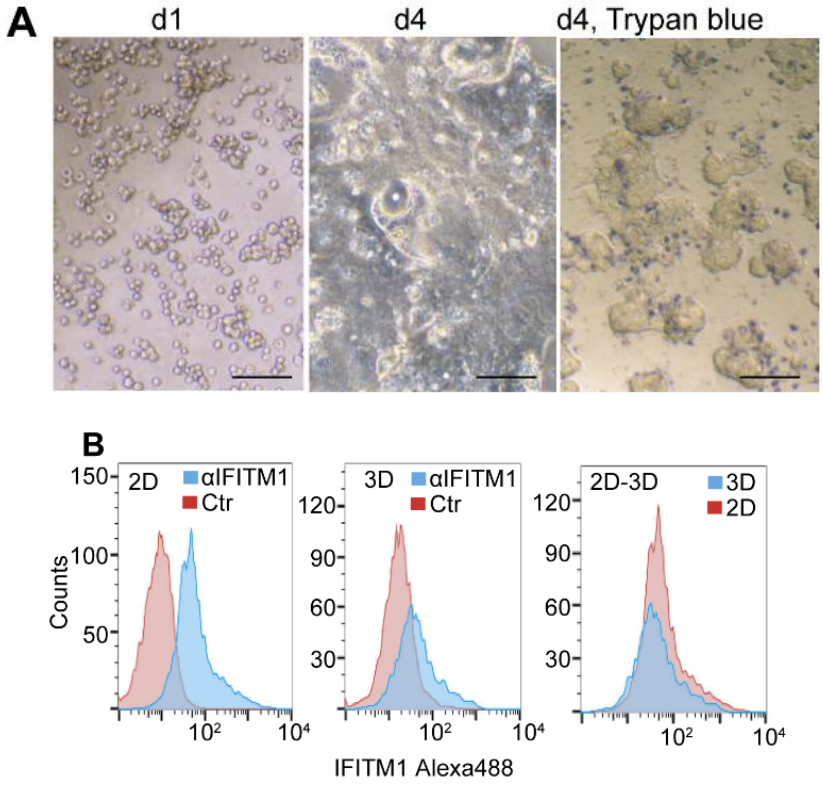

Figure 21: *CRC organoids are viable in 2D and they do not alter their IFITM1 expression level* ***A****: CRC organoids were dissociated into single cells and were plated to Matrigel-coated surfaces. Brightfield photo on day1 and day4. Trypan blue staining was carried out on day4. Scale bar: 50µm.* ***B****: Flow cytometric analysis of IFITM1 expression in 2D and 3D conditions. Note that only secondary antibody was used for control (ctr).*

Importantly, sorted cells maintained their IFITM1^{high} or IFITM1^{low} expression patterns at day 7, determined by RT-qPCR (**Fig. 22A**). Furthermore, IFITM1^{high} CRC cells showed a higher IFITM1 expression by immunocytochemistry even after 3 or 7 days in 2D and

3D cultures, respectively (**Fig. 22B**). Thus, the pattern of IFITM1 expression is maintained both in short-term 2D and 3D cultures.

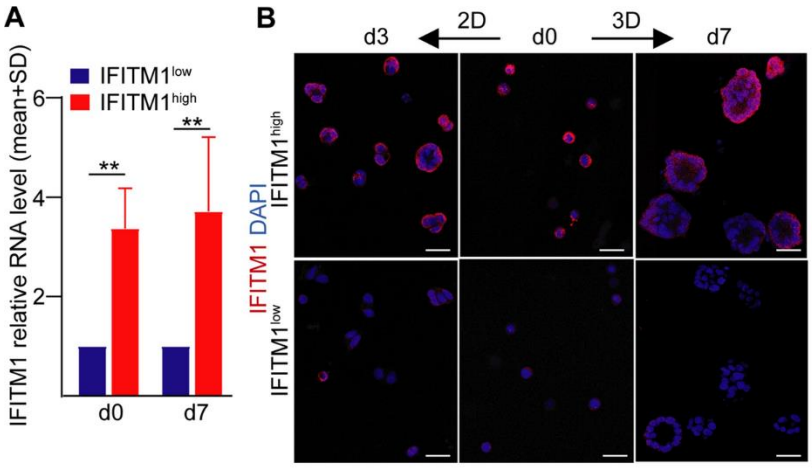

Figure 22: *IFITM1 sorted CRC cell-derived organoids maintain the expression difference* ***A****: Gene expression analysis of the IFITM1 sorted cells at day0 and day7. Data were normalized to the GAPDH gene. IFITM^{low} subpopulation was taken as 1. Statistical analysis: paired t-test. ** p < 0.01* ***B****: Whole-mount immunocytochemistry of the IFITM1 sorted cell-derived organoids in 2D and 3D conditions at day0, day3, or day7. Scale bar: 50µm*

Based on a previous study from our research group, small EVs (sEV, with a diameter of 50–100 nm) are preferentially released from 3D cultures into the medium (*58*). sEVs can be captured from the organoid supernatants by anti-CD63 or anti-CD81-coated beads and the percentage of positive beads can be detected by flow cytometry, providing a semi-quantitative method to compare EV concentrations (*58, 68*).

When comparing the sEV release from IFITM1^{high} and IFITM1^{low} cell-derived organoids, we found no difference in the sEV concentration between the two sorted cell population-derived organoids either with the bead-based semi-quantitative method or with NTA (**Fig. 23A-D**).

DOI:10.14753/SE.2022.2728

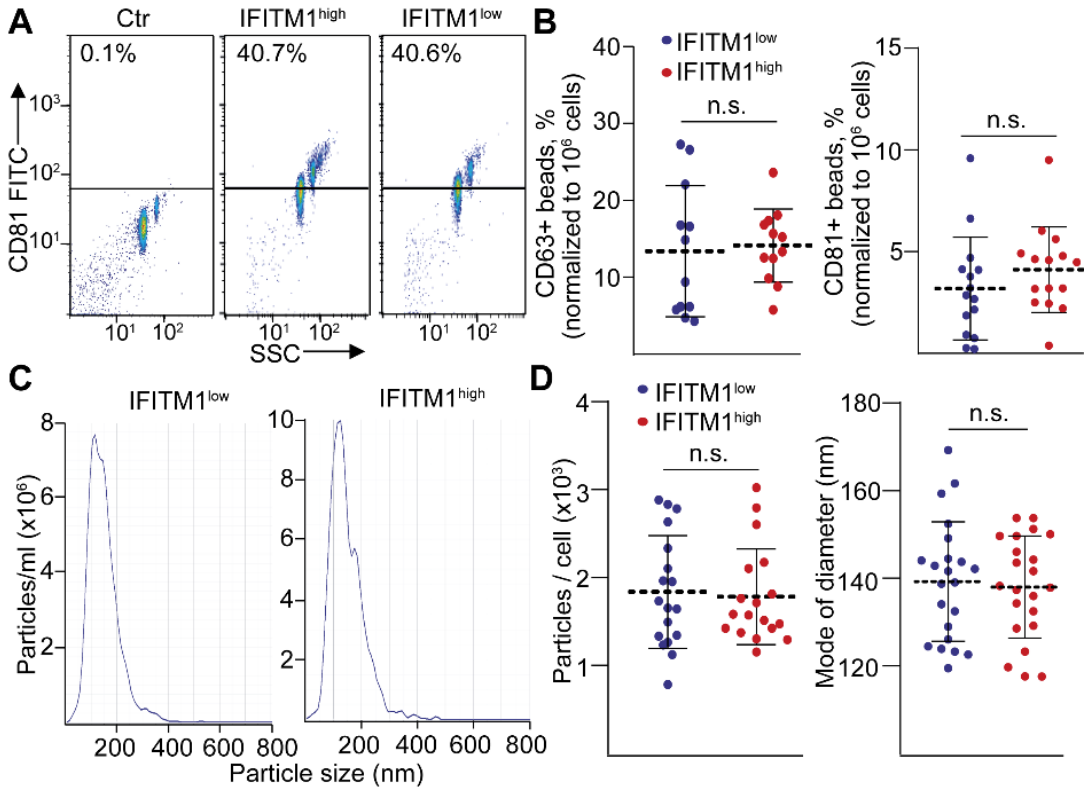

Figure 23*: There is no EV release difference between the IFITM1 subpopulations in Matrigel* ***A****: Representative images of the measurements with the bead-based semiquantitative method (CD81+ EVs were detected). The samples were collected from organoid supernatants.* ***B****: The percentage of CD63+ or CD81+ beads normalized by cell number. Data were obtained from the supernatant of the sorted organoid cells in Matrigel culture on day7. Statistical analysis: Mann–Whitney U test. n.s.>0.05.* ***C****: The diameter distribution of sEVs from IFITM1 sorted organoid line conditioned media by using NTA* ***D:*** *The particle number in the IFITM1 sorted organoid supernatants, normalized by cell number (left). The particle diameter in IFITM1 sorted organoid supernatants.*

We obtained similar data when sorted cells were cultured in another matrix, collagen I, or in a mixture of collagen I and Matrigel (**Fig. 24A-B**). These results suggest that IFITM1^{high} and IFITM1^{low} CRC cells do not have an altered release of sEVs.

DOI:10.14753/SE.2022.2728

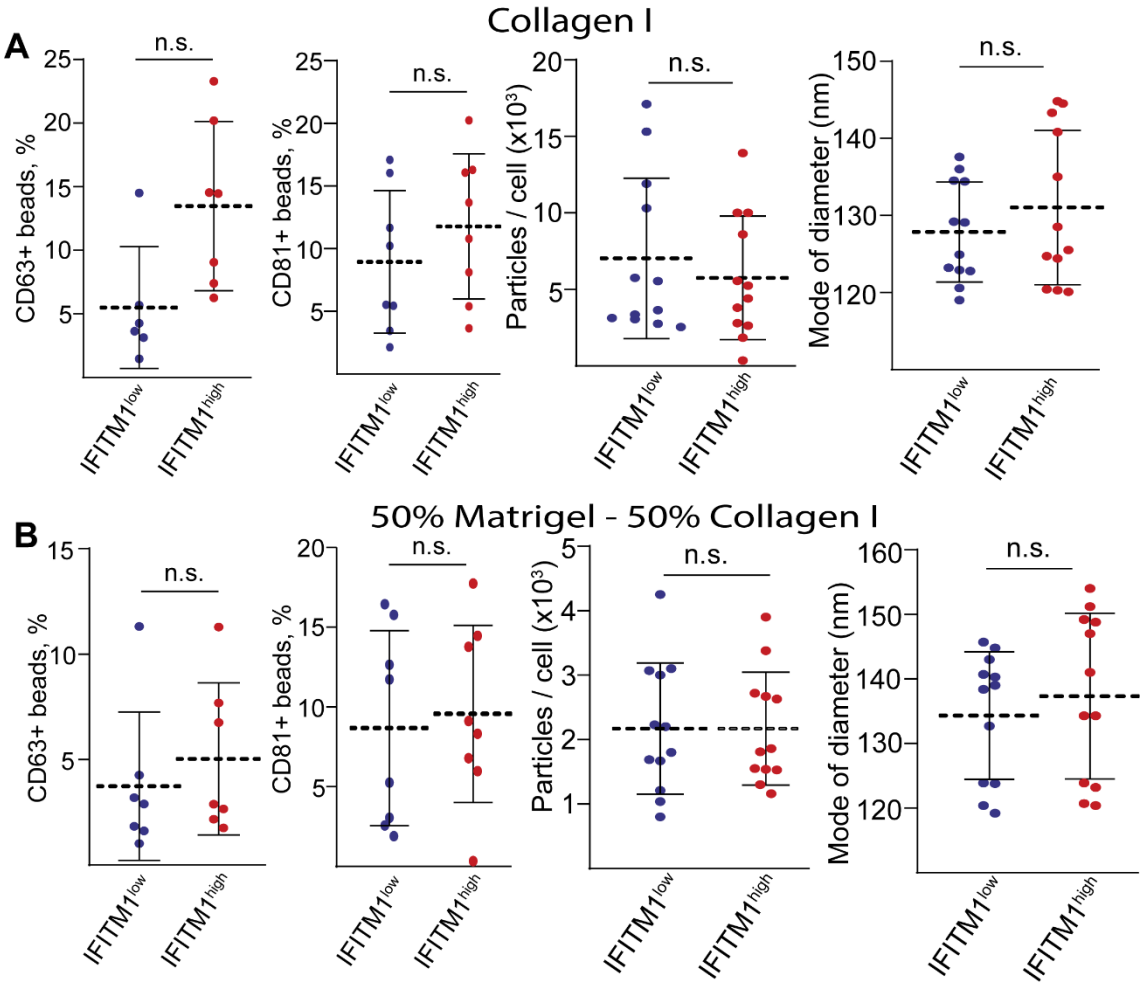

***Figure 24**: There is no EV release difference between the IFITM1 subpopulations in different matrices **A, B**: The percentage of CD63+,r CD81+ beads normalized by cell number (left two panels). The particle number in the IFITM1 sorted organoid culture supernatants, normalized by cell number and the particle diameter in IFITM1 sorted organoid supernatants (right two panels). The data were derived from the supernatant of the IFITM1 sorted organoids in (A) collagen or (B) 50% Matrigel/50% collagen I mixture culture at day7. Statistical analysis: Mann–Whitney U test. n.s. $p > 0.05$. .*

3.8. IFITM1^{high} CRC cells take up less EVs

Next, we studied whether cell populations with different Ifitm1 expression levels have different EV uptake abilities. To address this question, we cultured cells from WT and *Apc* mutant mouse intestinal organoids in 2D conditions for the short term and we added EVs isolated by centrifugation at 12,500g (medium EV fraction, mEV) from fibroblasts that had been pre-treated with a membrane labeling dye (**Fig. 25A**). Importantly, we found no increase in the percentage of active caspase+ cells after labeling, showing that this treatment did not induce apoptosis in fibroblasts (**Fig. 25B**). Since EVs were not directly labeled and cells were washed after applying the dye, this precluded the

possibility that we measured only dye aggregates. Importantly, we detected EVs in fibroblast culture supernatant by NTA measurements when isolating mEVs or sEVs (**Fig. 25C**). Furthermore, TEM proved the identity of EVs in samples after ultracentrifugation (**Fig. 25D**). In addition, capillary-based immunoblot showed the presence of the sEV marker TSG101 only in sEV preparations, whereas we could detect calnexin in the mEV fraction (**Fig. 25E**)(*69*).

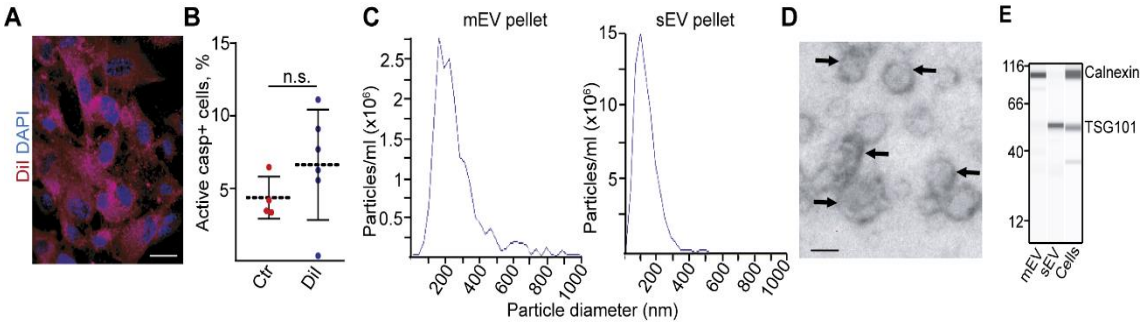

***Figure 25**: The membrane dye does not alter the viability of the fibroblasts **A**: Representative confocal image of DiI labeled normal colon fibroblasts (DiI: membrane labelling dye). Scale bar: 50μm **B**: The percentage of active caspase-3+ cells in DiI labeled colon fibroblast. The quantification was based on confocal microscopic images. Statistical analysis: Mann–Whitney U-test, n.s. p > 0.05 **C**: Representative curves from NTA measurements. EVs were isolated from colon fibroblast conditioned media. mEV was produced from the 12,500g pellet, sEV was obtained from the pellet after ultracentrifugation **D**: TEM images from ultracentrifuged colon fibroblast supernatant. Scale bar: 100nm **E**: Capillary-based WES immunoblot analysis of isolated sEV and mEV samples from fibroblast cell line. Fibroblast cell lysates were used as control*

Interestingly, Apc mutant organoids that expressed a higher level of Ifitm1, accumulated less fibroblast-derived mEVs compared to wild-type intestinal organoids (**Fig. 26**).

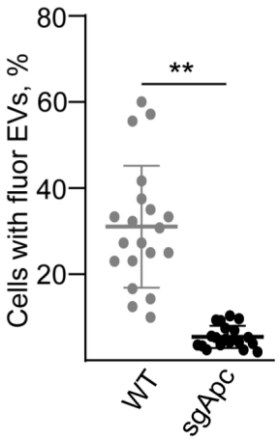

***Figure 26**: Apc mutant mouse organoids take up less EVs than WT colon organoids. The percentage of DiI labeled EV positive mouse colon wild type (WT) and Apc mutant (sgApc) organoid cells. Statistical analysis: Mann–Whitney U-test, **p<0.01*

To study whether EV uptake intensity differs between CRC cell subpopulations as well, we next sorted IFITM1^{high} and IFITM1^{low} cells and we cultured them with labeled mEVs or sEVs. Of note, less IFITM1^{high} cells took up EVs both in the case of HT29 CRC cell-line-derived and human colon fibroblast-derived mEVs as compared to IFITM1^{low} CRC cells, detected by confocal microscopy (**Fig. 27A-B**). In addition, IFITM1^{high} cells that had taken up fibroblast-derived EVs showed a lower signal intensity for mEVs than IFITM^{low} cells (**Fig. 27C**). Thus, these results suggest that the difference in EV uptake is not restricted to one specific cell type-derived EVs. Importantly, we proved the presence of mEVs and sEVs in the conditioned medium of HT29 cells with NTA and transmission electron microscopy (**Fig. 27D-E**). In addition, when samples were treated with Triton X-100 which disrupts biological membranes, the EV signal disappeared from the cells (**Fig. 27F**), proving that we visualized membrane-enclosed EVs in our experiments. Interestingly, this was not observed with saponin which is a less powerful detergent and disrupts only the external membranes (such as plasmamembrane) but not the membranes of the endo-lysosomal compartment.

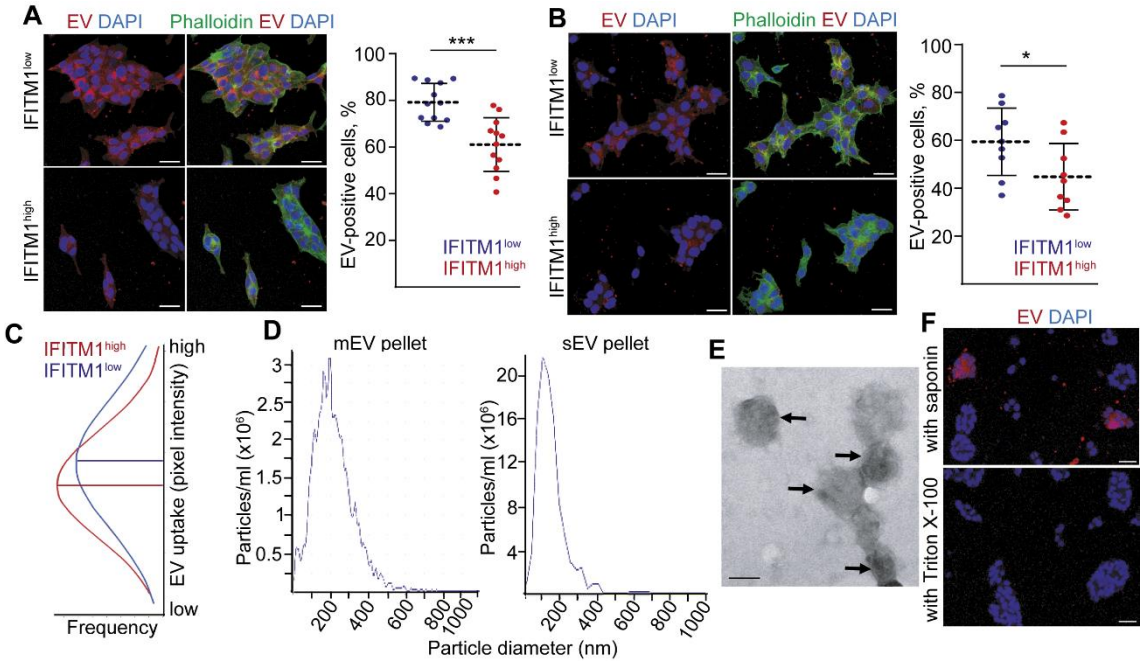

***Figure 27**: IFITM1^{low} cells take up more EVs than IFITM1^{high} cells **A, B**: Medium EV (mEV) uptake in IFITM1^{low} and IFITM1^{high} sorted cells. Representative images (left panels) and their quantification (right panels). Sorted cells were cultured 2D for 3 days and they were treated with mEVs derived from DiI-labelled HT29 CRC cells (A) or human colon fibroblasts (B). Note that mEVs show red fluorescence and phalloidin was used to visualize cells. The shown images are optical slices. Scale bars: 20 µm, statistical analysis: Mann–Whitney U-test, * $p < 0.05$, and *** $p < 0.005$ **C**: Distribution of the DiI signal intensity in IFITM1^{low} and IFITM1^{high} cells. Cells were treated with mEVs derived from*

DiI-labelled fibroblasts. Note the shift of the curve between the two cell populations ***D****: Representative curves from NTA measurements. EVs were isolated from HT29 conditioned media. mEVs were derived from the 12,500g pellet and sEVs from the pellet after ultracentrifugation.* ***E****: TEM images from ultracentrifuged HT29 supernatant. Scale bar: 100nm* ***F****: The fluorescent red signal of mEVs in IFITM1^{low} sorted cells, cultured for 3 days in 2D conditions. mEVs were collected from DiI-labelled fibroblasts and samples were treated with saponin or Triton X-100. Note that the EV signal disappears when using Triton X-100*

As the next experiment, we treated CRC organoid cells with fibroblast-derived labeled EVs in 2D cultures and then sorted cells with the highest and lowest fluorescent signal, representing cell populations with high and low EV uptake ability, respectively (**Fig. 28A**). Whereas we found no difference in the expression of *AXIN2* and *MYC*, we measured a significantly higher RNA level of *IFITM1* in cells with low EV uptake (**Fig. 28B**). Since we found no increase in the expression of *IFITM1* in CRC cells after treatment with EVs (**Fig. 28C**), this confirms again that IFITM1^{high} cells take up less EVs. In addition, the majority of cells with high IFITM1 levels were negative for the fluorescent signal after treatment with labeled fibroblast-derived mEVs. Furthermore, we observed the accumulation of IFITM1^{low} cells within the mEV+ cell population, measured by flow cytometry (**Fig. 28D**). When focusing on cells that had taken up mEVs, we detected a higher signal intensity, characterizing a higher mEV uptake, within the IFITM1^{low} cell population (**Fig. 28E**). Importantly, we obtained similar results when CRC organoid cells were treated with the sEV fraction collected from labeled fibroblasts or HT29 cells (**Fig. 28F**). Collectively, all these data prove i) the presence of cell subclones in CRC with different mEV and sEV uptake ability and ii) that IFITM1^{high} marks cells with a lower EV uptake.

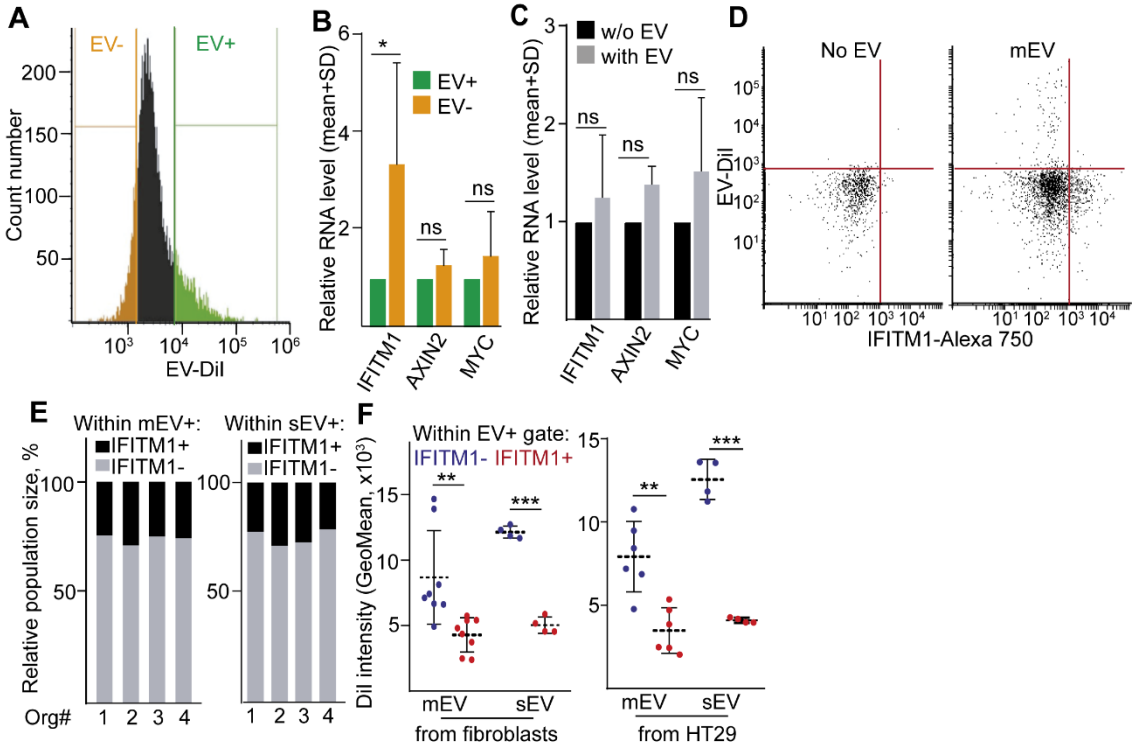

***Figure 28**: The EV^{negative} CRC cell subpopulation expresses IFITM1 at a higher level **A**: The fluorescence sorting strategy for the EV uptake capability (DiI signal intensity) **B**: Gene expression analysis of the EV^{positive} and EV^{negative} CRC cell subpopulations. Data were normalized to the GAPDH gene. Values from the EV^{positive} subpopulation were taken as 1. Statistical analysis: paired t-test. * $p < 0.05$, n.s. > 0.05 **C**: Gene expression analysis of the EV treated and untreated CRC organoids. Data were normalized to the GAPDH gene. The untreated sample was taken as 1. Statistical analysis: paired t-test. n.s. > 0.05 **D**: Representative dot plots from flow cytometric analysis of the CRC organoids with/without DiI labeled mEV treatment. IFITM1 level (x-axis) and EV signal intensity (y-axis) are shown. The lines show the signal intensity with the secondary control antibody. **E**: The quantification of flow cytometric analysis. The relative percentage of IFITM1^{high} and IFITM1^{low} cells within cells with mEV (left panel) or sEV (right panel) in four CRC organoid lines (flow cytometry) are shown. **F**: The quantification of flow cytometric analysis. EV-DiI red fluorescent signal intensity in IFITM1$^{-/low}$ and IFITM1^{high} cells after treatment with mEVs or sEVs isolated from fibroblasts (left panel) or HT29 cells (right panel). Statistical analysis: Mann–Whitney U-test, ** $p < 0.01$, and *** $p < 0.005$*

3.9. Fibroblast-derived EVs result in a marked increase in the proliferating cell number of IFITM1^{low} CRC organoids

To test the functional relevance of differential EV uptake between CRC cell subpopulations, we first added fibroblast-derived mEVs or sEVs to CRC cells and we then detected IFITM1 expression and KI67 in the organoids after 7 days. Importantly, neither sEVs nor mEVs resulted in a change in the percentage of IFITM1+ CRC cells (**Fig. 29A**). However, we detected a markedly higher increase in the proportion of proliferating cells within the IFITM1- cell population than in IFITM1+ cells in the

presence of EVs (**Fig. 29A**). Furthermore, adding fibroblast-derived mEVs or sEVs to sorted IFITM1^{low} cells resulted in organoids with a markedly higher increase in the number of KI67+ cells as compared to IFITM1^{high} cell-derived organoids (**Fig. 29B**). In addition, the initial difference in the percentage of proliferating cells between the two CRC cell subpopulations disappeared after treatment with mEVs or sEVs (**Fig. 29C**). On the other hand, we detected no changes in the percentage of active caspase-3+ apoptotic cells (**Fig. 29D**). Thus, these results indicate that differential mEV or sEV uptake by CRC cell subpopulations critically modified the percentage of proliferating cells in an organoid model.

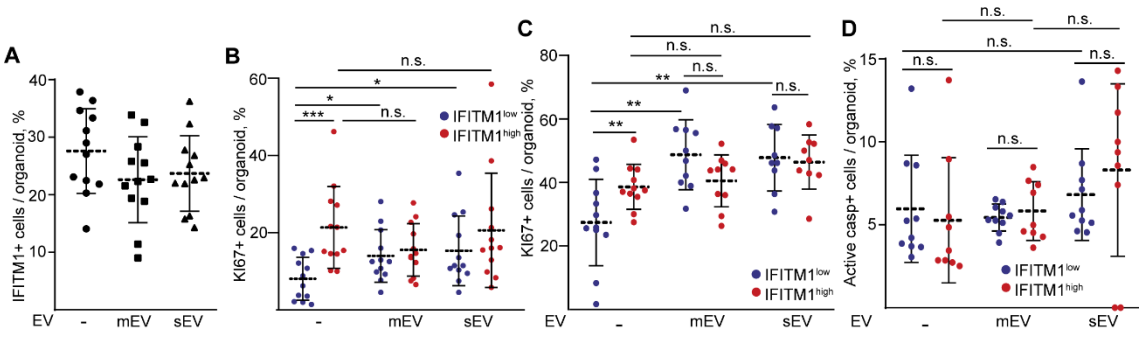

***Figure 29**: IFITM^{low} CRC cells are more responsive to EV treatment **A**: The percentage of IFITM1+ cells without and after mEV or sEV treatment. The quantification was carried out on confocal microscopic images. **B**: The percentage of IFITM1^{low}/KI67+ and IFITM1^{high}/KI67+ cells in CRC organoids after the indicated treatments. The quantification of confocal microscopic images. Statistical analysis: two-way ANOVA, and Tukey post hoc tests, * $p < 0.05$, *** $p < 0.005$, n.s. > 0.05 **C**: The percentage of KI67+ proliferating cells in IFITM1^{high} or IFITM1^{low} CRC cell-derived organoids, treated with fibroblast sEVs or mEVs directly after sorting. The quantification was based on confocal microscopic images. Statistical analysis: two-way ANOVA, and Tukey post hoc tests, ** $p < 0.01$, n.s. > 0.05 **D**: The percentage of active caspase-3+ cells in IFITM1^{high} or IFITM1^{low} CRC cell-derived organoids, treated with fibroblast sEVs or mEVs directly after sorting. Statistical analysis: two-way ANOVA, and Tukey post hoc tests, n.s. > 0.05*

3.10. Deleting IFITM1 results in a higher EV uptake in CRC organoid cells

To test whether IFITM1 is functionally important for the enhanced proliferation rate and reduced EV uptake of cells with IFITM1^{high} expression, we inactivated this gene in CRC organoids by the CRISPR/Cas9 system. The plasmids were introduced into the cells by nucleofection using the 4-D Nucleofector (Lonza) intrument. After 14 days of selection for the genetically modified cells, flow cytometry and immunocytochemistry proved the largely diminished level of IFITM1 in these cells (**Fig. 30A-B**). Of note, we observed a decreased diameter of organoids established from IFITM1^{KO} cells (**Fig. 30C**). When using labeled human colon fibroblast EVs, we detected a markedly higher percentage of

EV-positive cells derived from IFITM1^{KO} organoids compared to IFITM1^{WT} cells (**Fig. 30D**), indicating that the lack of IFITM1 induced EV uptake. Similar to the IFITM1^{low} and IFITM1^{high} populations, IFITM1^{KO} organoids showed a reduced percentage of KI67+ cells compared to IFITM1^{WT} organoids (**Fig. 30E**). However, fibroblast-derived mEVs or sEVs had a larger effect on the proliferation of IFITM1^{KO} organoids (**Fig. 30E**), indicating the functional effect of the increased EV uptake of cells without IFITM1. Collectively, these data suggest that IFITM1 is not only a marker of a CRC cell population with reduced EV uptake ability, but this molecule is also functionally involved in this process.

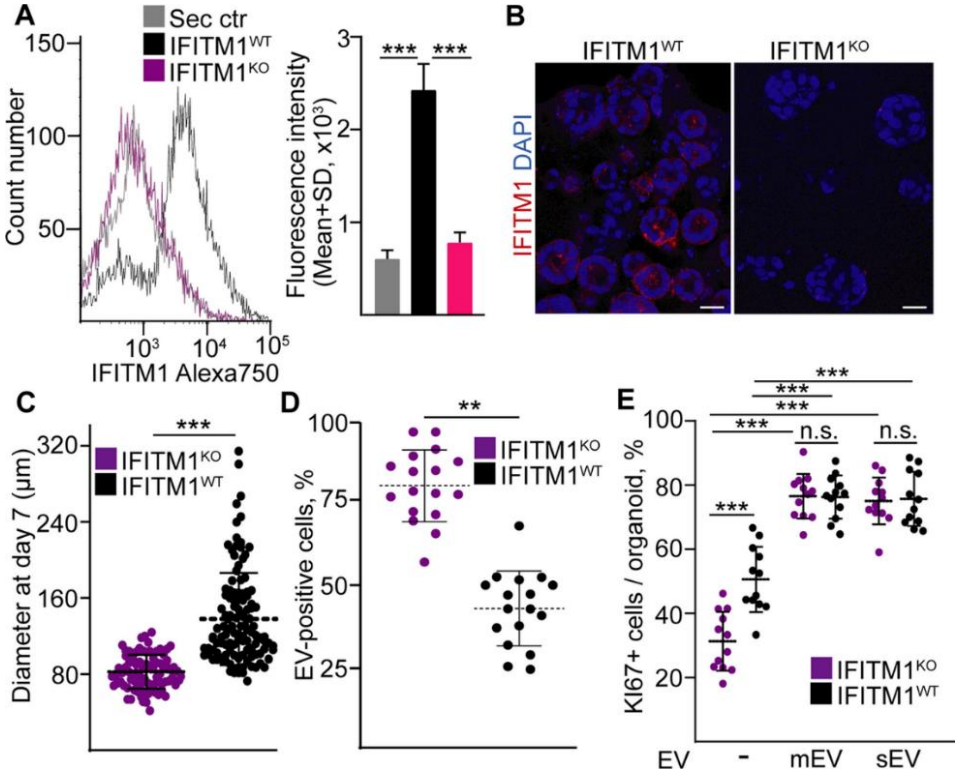

***Figure 30**: IFITM1^{KO} has the same EV uptake pattern as the IFITM11^{low} subpopulation **A**: Flow cytometric analysis of IFITM1 expression in IFITM1^{WT} and IFITM1^{KO} cells. Sec ctr: control with only secondary antibody. Representative histogram (left) and the quantification (right) (GeoMean values were analyzed). Statistical analysis: unpaired t-test, *** $p < 0.005$. **B**: Whole-mount immunocytochemistry of IFITM1 on samples with/without IFITM1 inactivation. Scale bar: 50 µm. **C**: The diameter of the IFITM1^{WT} and IFITM1^{KO} organoids at day7 after replating. Statistical analysis: Mann–Whitney U-test, ** $p < 0.01$ **D**: The percentage of the EV positive cells in IFITM1^{WT} and IFITM1^{KO} CRC 2D cultures. Statistical analysis: Mann-Whitney U-test, ** $p < 0.01$ **E**: The percentage of KI67+ CRC cells after mEV or sEV treatment. The quantification used confocal microscopic images. Statistical analysis: Kruskal–Wallis and Dunn tests, *** $p < 0.005$, n.s. > 0.05*

4. Discussion

Colorectal cancer (CRC) is one of the most prevalent cancer types. In addition, its high mortality rate also highlights the importance of examining this public health problem (*70*). In our projects, we studied the intratumoral heterogeneity of CRC and its influence on paracrine tumor-stroma communication. Intratumoral heterogeneity is a commonly overlooked hallmark of cancer that causes major difficulties in the treatment. (*29*) It is a well-known fact that the tumor itself is not just the plurality of the cells. It has several cell types next to the cancer cells, such as fibroblasts, immune cells, and endothelial cells. Interestingly, there are subpopulations with different functions among cancer cells. (*71*) However, this functional heterogeneity was not well described just in a few cases yet, for example, LGR5 and PROX1 positive cells hold stem-like cell features, although these subpopulations only partially overlap. (*32, 33*) My dissertation focuses on cell surface molecules that mark aggressive CRC cell populations in CRC, CD44, CD133, and PTK7. CD44 is a hyaluronic acid receptor and marks an invasive cell type in CRC (*35*). CD133, also called Prominin-1 is the first identified stem cell marker (*37*). PTK7 is an inactive receptor tyrosine kinase and a study proved that PTK^{+} cells show different chemosensitivity compared to the PTK^{low} subpopulation in cancer cell lines (*39*). We proved that among these invasive cell markers only $CD44^{high}$ CRC cells release a significantly higher amount of EVs compared to the $CD44^{low}$ CRC cells. As the next step, we examined the miRNA cargo of the released EVs by the different subpopulations.

MicroRNAs (miRNAs) are widely studied non-coding RNAs with an average of 22nt length that play a regulating role in gene expression. The majority of the miRNAs have several processing steps (primary-miRNAs, precursor-miRNAs) to finally become matured miRNAs. Numerous studies described miRNAs interacting with the 3'UTR region of the target mRNA (*72*), however, others proved interactions with the 5'UTR, coding sequence, and gene promoters as well (*73*). miRNAs can also activate translation in special situations or regulate transcription. They can be secreted to the extracellular space and transported to the target cells by binding to proteins such as Argonaute or by a protected way in EVs (*74*). Although a sorting mechanism has been identified for EV miRNAs based on sequence motifs, not all EV miRNAs contain these sequences. However, the sorting of miRNAs does not seem to be a stochastic procedure but is driven by other pathways as well. The extracellular miRNAs have a chemical messenger

function to mediate cell-cell communication. By this feature, the EV miRNAs are potential diagnostic and prognostic biomarkers and participate in pre-metastatic niche formation, metastatic tumorigenesis, and therapy resistance (*75*).

Although the level of released EVs differs between $CD44^{high}$ and $CD44^{low}$ CRC cells, the miRNA cargos show only a modest difference between these subpopulations. 26 common miRNAs were detected in EVs derived from either $CD44^{high}$ or $CD44^{low}$ CRC cells. According to a meta-analysis, the majority of the detected miRNAs were present also in the plasma samples of CRC patients compared to healthy controls (*76*). We detected miR-95, miR-100, and miR-365 in EVs derived from the $CD44^{high}$ cell population when sorting cells based on differential CD44 expression. miR-95 was shown to induce cell proliferation by suppressing sorting nexin1 (SNX1) expression in CRC (*77*). miR-100 mediates cetuximab resistance by increasing the strength of Wnt signaling (*78*). In addition, this miR inhibited cell proliferation in multiple systems, such as in CRC (by decreasing Lgr5 expression (*79*)) or mammary tumor cells both *in vitro* and *in vivo* (*80*). Similarly, miR-365 is frequently down-regulated in CRC. It inhibits cell cycle progression and induces apoptosis (*81*). Interestingly, miR-365 has a contradictory role in different cancer types and some reports showed it having promoting, while others showed inhibiting effects on cell proliferation (*82–84*). Importantly, miR-365 was also suggested as a biomarker in oral squamous cell carcinoma-derived EVs (*85*). The only miR that we found to be specific for $CD44^{low}$ CRC cell-derived EVs was miR-345 which is known to stimulate cell proliferation and invasion (*85*).

EVs induced the activation and proliferation of fibroblasts and we proved that this process was dose-dependent. Next, we used artificial liposomes to examine whether fibroblast activation was based on the miRNA content or the EV dose. These particles were produced from phosphocholine and cholesterol with no miRNA or protein cargos. We obtained the same dose-dependent fibroblast activation as for EVs, raising the possibility that the lipid components of EVs are the active components. This observation is supported by the work showing that cholesterol-induced many functions of prostate cancer cells, such as proliferation and migration (*86*). Furthermore, cell-intrinsic and cell-extrinsic cues, reprogram cholesterol metabolism in multiple tumors and promote tumorigenesis (*87*). In addition, lipid uptake can induce the proliferation of not only cancer cells, but of

fibroblasts as well (*88*). Further experiments are needed to clarify the mechanisms of how the lipid components of EVs and liposomes act in fibroblasts.

As another approach, we identified IFITM1 as a marker for an aggressive CRC cell subpopulation. We proved that after *APC* mutation, which is one of the most common driver mutations in CRC, the level of IFITM1 increased more than 2,500 fold. This elevation was detectable in patient-derived samples as well. Importantly, IFITM1 is critical in virus uptake. Since EVs can be edited and loaded with specific molecules and are considered as a promising tool for targeted cancer therapy, we examined whether cells with differing IFITM1 levels take up a different amount of EVs. We proved that IFITM1^{high} CRC cells take up less EVs compared to IFITM1^{low} CRC cells. Of note, deleting IFITM1 led to the marked increase in EV uptake, proving that IFITM1 is not only a marker of a CRC cell population, but is also actively involved in this process. Fibroblast-derived EVs resulted in a marked increase in the proliferating cell number of IFITM1^{low} CRC organoids, showing the functional significance of the difference in EV uptake. We also showed that *Ifitm1* expression is increased after *Apc* mutation, similarly to human adenomas when compared to normal colonic epithelium. CRC patient-derived organoids had a heterogeneous intra-organoid expression of *IFITM1* and the IFITM1^{high} CRC population contained more proliferating cells.

IFITM family members have been identified as molecular markers in human colorectal tumors (*89*). A few studies have also demonstrated the connection of IFITM1 to the progression of CRC, showing that it modifies the proliferating, invasive, and metastatic capability of CRC cell lines (*90*). However, the majority of these previous data were derived from models using cell lines cultured 2D. Importantly, we were the first who used patient-derived organoids to characterize IFITM1^{high} CRC cells. We observed that IFITM1^{high} sorted cells formed organoids with more proliferating cells, suggesting that IFITM1^{high} and IFITM1^{low} subpopulations differentially contributed to CRC tumorigenesis. Interestingly, we found no difference in the RNA level of some CRC stem cell and Wnt target genes, indicating that IFITM1 may regulate proliferation not directly via the Wnt pathway. In line with these data, loss of IFITM1 markedly increased nuclear p21 level, leading to reduced proliferation in breast cancer (*91*). Another study found that targeting IFITM1 inhibited the proliferation of breast cancer cells via NFκB (*92*).

IFITM genes are generally regulated by type I and type II interferons. We proved here that human organoids derived from adenomas or CRC patients expressed IFITM1 at a higher level compared to the normal colon. By using genetically modified mouse intestinal organoids, we provided evidence that *Apc* mutation was a critical factor in the regulation of *Ifitm1* expression. Our findings concur with the results of Lickert et al (*93*) who found a regulatory effect of the Wnt pathway on *Ifitm* genes during gastrulation. In addition, we confirmed the results by Andreu et al. (*94*), showing the regulation of many *Ifitm* members in mouse intestinal adenoma models. However, we found no difference in IFITM1 expression in the $LGR5^{high}$ CRC cells compared to $LGR5^{low}$ cells. Although $LGR5^{high}$ cells represent a CRC cell population with stem cell features and high Wnt activity (*31*), this finding suggests that IFITM1 expression is regulated not only by the strength of the Wnt activation, but other signaling pathways may have a critical influence as well.

The *IFITM* genes encode for a group of small homologous proteins that are localized in the membranes of the endosomal-lysosomal compartment or the plasma membrane (*95*). IFITM proteins provide a cellular resistance against a wide variety of both enveloped and non-enveloped viruses not only *in vitro* but *in vivo* as well (*96, 97*). Similar to certain viruses, EVs contain a membrane envelope. Although the mechanism of action of the IFITM proteins is largely unknown, some studies suggested that they exert their anti-viral effects via modifying the fluidity or other physicochemical properties of biological membranes (*98, 99*) which may be the mechanism for the differential EV uptake as well. Of note, here we show that $IFITM1^{high}$ cells take up less EVs compared to cells with low IFITM1 expression. Thus, our results indicate the existence of differential EV uptake within CRC. Furthermore, by inactivating IFITM1, we also demonstrated that this molecule was functionally important for this process. Thus, these data provide further evidence for the relationship between certain viruses and EVs not only in the mechanism of their production but in their uptake as well (*100*). Of note, the $IFITM1^{low}$ population contained less proliferative cells compared to the $IFITM1^{high}$ population. However fibroblast-derived EVs diminished this difference between $IFITM1^{high}$ and $IFITM1^{low}$ cells. They had a more pronounced stimulatory effect on cell proliferation in the $IFITM1^{low}$ CRC subpopulation that accumulated more EVs. These data not only highlight

the complex regulation of proliferation in CRC but also illustrate the biological importance of the differential EV uptake by tumor cells.

EVs contain proteins in their membranes that enhance their uptake, thus, providing a powerful delivery system of drugs or RNAs in RNA interference (RNAi)-based approaches. The usability of this approach has recently been proven by two elegant studies. In these publications, RNAi was delivered to specifically target the oncogenic KRas in pancreatic tumors in mouse models (*101*, *102*). Importantly, these results open the possibility for engineered EV-based therapies targeting oncogenes in other cancers, such as in CRC. However, the proper and efficient use of EVs delivering the engineered cargo critically depends on their uptake by tumor cells. Importantly, the heterogeneous level of IFITM1 on CRC cells may result in the diminished efficiency of EV-mediated drug delivery in some CRC cell subpopulations. Furthermore, the *Apc* mutation-induced Ifitm1 expression and the higher level of IFITM1 in CRC cells compared to normal colon epithelial cells raise the possibility that normal colon epithelial cells may be targeted even more efficiently by EVs than tumor cells.

DOI:10.14753/SE.2022.2728

5. Conclusions

Collectively, our results provide evidence that intratumoral heterogeneity is a key factor in tumor-stroma communication in CRC. Differential CD44 level marks CRC cell subpopulations with differing EV secreting capacity. Interestingly, $CD44^{high}$ and $CD44^{low}$ cell derived EVs have only modestly different miRNA cargos. We also proved that organoid derived EVs may induce the activation of fibroblasts. However, when comparing the effect of EVs from $CD44^{high}$ and $CD44^{low}$ CRC cells on fibroblasts, we found that the different EV number is the relevant factor, and we found no evidence for the importance of the miRNA cargo. These results may significantly contribute to understanding how EVs released from CRC subpopulations act in the tumor microenvironment.

Furthermore, we identified IFITM1 gene with an expression increase of more than 2,500 fold after *APC* mutation. When comparing CRC cell subpopulations with different IFITM1 levels, we found a higher proliferation capacity in case of $IFITM1^{high}$ CRC cells. In addition, differential IFITM1 levels marked CRC cells with largely differing EV uptake capacity. Although $IFITM1^{low/neg}$ cells had a lower proliferation potential, this subpopulation was more responsive to EV treatment, thus, EVs exerted a more pronounced effect in these cells compared to the $IFITM^{high}$ cells. By inactivating the IFITM1 gene we observed a similar EV uptake pattern compared to $IFTM1^{low}$ cells, thus, providing evidence that IFITM1 plays a functional role in EV uptake. Thus, IFITM1-regulated EV uptake intensity is a critical factor for modifying important tumorigenic features of some CRC cells, such as proliferation. Since this fact may influence the effect of EVs in clinical applications, it must be taken into consideration when designing EVs as therapeutic tools in CRC.

DOI:10.14753/SE.2022.2728

6. Summary

Extracellular vesicles (EV) are membrane-surrounded vesicles that are released by virtually all cell types and they participate in the intercellular communication. Since they carry biologically important molecules as cargo in a protected form and this cargo may reflect the molecular composition of the releasing cells, they are potential tools for targeted therapy and for tumor diagnostics. Colorectal cancer (CRC) is one of the most common cancers. The importance of the intratumoral heterogeneity of cancer cells is not yet fully understood, and, similarly, its impact on the intensity of EV release and uptake is still largely unknown. Patient-derived 3D organoids are one of the most modern methods to study this heterogeneity *in vitro*. When focusing on molecules that mark CRC cell subpopulations with an aggressive behavior, we detected an increased EV release by $CD44^{high}$ CRC cells. We found that the miRNA cargos of $CD44^{high}$ and $CD44^{low}$ cell-derived EVs largely overlapped and only four miRNAs were specific for one of the subpopulations. EVs released by $CD44^{high}$ cells induced the proliferation and activation of colon fibroblasts stronger than $CD44^{low}$ cells. This effect was not coupled to the miRNA cargo of the EVs, but to the higher EV release from $CD44^{high}$ CRC cells.

IFITM1 plays a critical role in virus uptake, thus, it was a candidate molecule that could modulate EV uptake. We observed a higher expression of IFITM1 in adenomas and CRCs compared to the normal colon. We proved that *Ifitm1* expression was at least partially regulated by *Apc* deletion which is a critical mutation in CRC patients. $IFITM1^{high}$ CRC cells had a higher proliferative potential. $IFITM1^{low}$ CRC cells took up more EVs. Exposure of $IFITM1^{low}$ organoids to fibroblast-derived EVs resulted in a more pronounced increase in KI67+ cell number. Inactivating IFITM1 resulted in a smaller organoid size and a higher EV uptake ability compared to unmodified CRC samples. Our data indicate that intratumoral heterogeneity led to tumor cell subpopulations with different abilities for EV uptake. The different EV uptake modified the proliferation intensity of CRC cell subpopulations. IFITM1 not only marked CRC subpopulations but also played a functional role in EV uptake in CRC. Collectively, we identified CRC subpopulations with different EV releasing and uptake capabilities and we proved that this intratumoral heterogeneity has a functional role, too. We propose that intratumoral heterogeneity for EV uptake and release should be considered as a critical factor when designing targeted EV-based therapy in CRC.

7. References

1. M. G. Guren (2019) The global challenge of colorectal cancer. *Lancet Gastroenterol. Hepatol.* **4**, 894–895.

2. Y. Xi, P. Xu (2021) Global colorectal cancer burden in 2020 and projections to 2040. *Transl. Oncol.* **14**, 101174.

3. E. F. Fearon, B. Vogelstein (1989) A genetic model for Colorectal Tumorigenesis. *Cell*. **61**, 759–767.

4. H. Clevers (2013) The Intestinal Crypt, A Prototype Stem Cell Compartment. *Cell*. **154**, 274–284.

5. M. Malumbres, M. Barbacid (2003) RAS oncogenes: the first 30 years. *Nat. Rev. Cancer*. **3**, 459–465.

6. G. A. Hobbs, A. Wittinghofer, C. J. Der (2016) Selective Targeting of the KRAS G12C Mutant: Kicking KRAS When It's Down. *Cancer Cell*. **29**, 251–253.

7. M. Meng, K. Zhong, T. Jiang, Z. Liu, H. Y. Kwan, T. Su (2021) The current understanding on the impact of KRAS on colorectal cancer. *Biomed. Pharmacother.* **140**, 111717.

8. M. Zhao, L. Mishra, C.-X. Deng (2018) The role of TGF-β/SMAD4 signaling in cancer. *Int. J. Biol. Sci.* **14**, 111–123.

9. T. Fang, T. Liang, Y. Wang, H. Wu, S. Liu, L. Xie, J. Liang, C. Wang, Y. Tan (2021) Prognostic role and clinicopathological features of SMAD4 gene mutation in colorectal cancer: a systematic review and meta-analysis. *BMC Gastroenterol.* **21**, 297.

10. F. Kruiswijk, C. F. Labuschagne, K. H. Vousden (2015) p53 in survival, death and metabolic health: a lifeguard with a licence to kill. *Nat. Rev. Mol. Cell Biol.* **16**, 393–405.

11. A. Hafner, M. L. Bulyk, A. Jambhekar, G. Lahav (2019) The multiple mechanisms that regulate p53 activity and cell fate. *Nat. Rev. Mol. Cell Biol.* **20**, 199–210.

12. W. Feroz, A. M. A. Sheikh (2020) Exploring the multiple roles of guardian of the

genome: P53. *Egypt. J. Med. Hum. Genet.* **21**, 49.

13. Cancer Genome Atlas Network. (2012) Comprehensive molecular characterization of human colon and rectal cancer. *Nature*. **487**, 330–337.

14. M. Matano, S. Date, M. Shimokawa, A. Takano, M. Fujii, Y. Ohta, T. Watanabe, T. Kanai, T. Sato (2015) Modeling colorectal cancer using CRISPR-Cas9–mediated engineering of human intestinal organoids. *Nat. Med.* **21**, 256–262.

15. E. Vilar, J. Tabernero (2013) Molecular Dissection of Microsatellite Instable Colorectal Cancer. *Cancer Discov.* **3**, 502–511.

16. R. Dienstmann, L. Vermeulen, J. Guinney, S. Kopetz, S. Tejpar, J. Tabernero (2017) Consensus molecular subtypes and the evolution of precision medicine in colorectal cancer. *Nat. Rev. Cancer*, doi:10.1038/nrc.2016.126.

17. K. Li, H. Luo, L. Huang, H. Luo, X. Zhu (2020) Microsatellite instability: a review of what the oncologist should know. *Cancer Cell Int.* **20**, 16.

18. D. K. Rex, D. J. Ahnen, J. A. Baron, K. P. Batts, C. A. Burke, R. W. Burt, J. R. Goldblum, J. G. Guillem, C. J. Kahi, M. F. Kalady, M. J. O′Brien, R. D. Odze, S. Ogino, S. Parry, D. C. Snover, E. E. Torlakovic, P. E. Wise, J. Young, J. Church (2012) Serrated Lesions of the Colorectum: Review and Recommendations From an Expert Panel. *Am. J. Gastroenterol.* **107**, 1315–1329.

19. S. Kang, Y. Na, S. Y. Joung, S. Il Lee, S. C. Oh, B. W. Min (2018) The significance of microsatellite instability in colorectal cancer after controlling for clinicopathological factors. *Medicine (Baltimore).* **97**, e0019.

20. A. Sadanandam, C. A. Lyssiotis, K. Homicsko, E. A. Collisson, W. J. Gibb, S. Wullschleger, L. C. G. Ostos, W. A. Lannon, C. Grotzinger, M. Del Rio, B. Lhermitte, A. B. Olshen, B. Wiedenmann, L. C. Cantley, J. W. Gray, D. Hanahan (2013) A colorectal cancer classification system that associates cellular phenotype and responses to therapy. *Nat. Med.* **19**, 619–625.

21. F. De Sousa E Melo, X. Wang, M. Jansen, E. Fessler, A. Trinh, L. P. M. H. de Rooij, J. H. de Jong, O. J. de Boer, R. van Leersum, M. F. Bijlsma, H. Rodermond, M. van der Heijden, C. J. M. van Noesel, J. B. Tuynman, E. Dekker, F. Markowetz,

J. P. Medema, L. Vermeulen (2013) Poor-prognosis colon cancer is defined by a molecularly distinct subtype and develops from serrated precursor lesions. *Nat. Med.* **19**, 614–618.

22. J. Guinney, R. Dienstmann, X. Wang, A. de Reyniès, A. Schlicker, C. Soneson, L. Marisa, P. Roepman, G. Nyamundanda, P. Angelino, B. M. Bot, J. S. Morris, I. M. Simon, S. Gerster, E. Fessler, F. De Sousa E Melo, E. Missiaglia, H. Ramay, D. Barras, K. Homicsko, D. Maru, G. C. Manyam, B. Broom, V. Boige, B. Perez-Villamil, T. Laderas, R. Salazar, J. W. Gray, D. Hanahan, J. Tabernero, R. Bernards, S. H. Friend, P. Laurent-Puig, J. P. Medema, A. Sadanandam, L. Wessels, M. Delorenzi, S. Kopetz, L. Vermeulen, S. Tejpar (2015) The consensus molecular subtypes of colorectal cancer. *Nat. Med.* **21**, 1350–1356.

23. J.-Y. Kim, Y.-E. Cho, J.-H. Park (2015) The Nucleolar Protein GLTSCR2 Is an Upstream Negative Regulator of the Oncogenic Nucleophosmin-MYC Axis. *Am. J. Pathol.* **185**, 2061–2068.

24. P. D. Dunne, D. G. McArt, C. A. Bradley, P. G. O'Reilly, H. L. Barrett, R. Cummins, T. O'Grady, K. Arthur, M. B. Loughrey, W. L. Allen, S. S. McDade, D. J. Waugh, P. W. Hamilton, D. B. Longley, E. W. Kay, P. G. Johnston, M. Lawler, M. Salto-Tellez, S. Van Schaeybroeck (2016) Challenging the Cancer Molecular Stratification Dogma: Intratumoral Heterogeneity Undermines Consensus Molecular Subtypes and Potential Diagnostic Value in Colorectal Cancer. *Clin. Cancer Res.* **22**, 4095–4104.

25. Y. Zhang, X. Wang (2020) Targeting the Wnt/β-catenin signaling pathway in cancer. *J. Hematol. Oncol.* **13**, 165.

26. R. Nusse, H. Clevers (2017) Wnt/β-Catenin Signaling, Disease, and Emerging Therapeutic Modalities. *Cell*. **169**, 985–999.

27. B. L. LeSavage, R. A. Suhar, N. Broguiere, M. P. Lutolf, S. C. Heilshorn (2021) Next-generation cancer organoids. *Nat. Mater.* doi:10.1038/s41563-021-01057-5.

28. F. Caiado, B. Silva-Santos, H. Norell (2016) Intra-tumour heterogeneity - going beyond genetics. *FEBS J.* **283**, 2245–2258.

29. K. Hinohara, K. Polyak (2019) Intratumoral Heterogeneity: More Than Just Mutations. *Trends Cell Biol.* **29**, 569–579.

30. I. Dagogo-Jack, A. T. Shaw (2018) Tumour heterogeneity and resistance to cancer therapies. *Nat. Rev. Clin. Oncol.* **15**, 81–94.

31. C. Cortina, G. Turon, D. Stork, X. Hernando-Momblona, M. Sevillano, M. Aguilera, S. Tosi, A. Merlos-Suárez, C. Stephan-Otto Attolini, E. Sancho, E. Batllez (2017) A genome editing approach to study cancer stem cells in human tumors. *EMBO Mol. Med.* **9**, 869–879.

32. M. Shimokawa, Y. Ohta, S. Nishikori, M. Matano, A. Takano, M. Fujii, S. Date, S. Sugimoto, T. Kanai, T. Sato (2017) Visualization and targeting of LGR5+ human colon cancer stem cells. *Nature*. **545**, 187–192.

33. Z. Wiener, J. Högström, V. Hyvönen, A. M. Band, P. Kallio, T. Holopainen, O. Dufva, C. Haglund, O. Kruuna, G. Oliver, Y. Ben-Neriah, K. Alitalo (2014) Prox1 promotes expansion of the colorectal cancer stem cell population to fuel tumor growth and ischemia resistance. *Cell Rep.* **8**, 1943–1956.

34. A. Niida, K. Mimori, T. Shibata, S. Miyano (2021) Modeling colorectal cancer evolution. *J. Hum. Genet.* **66**, 869–878.

35. C. Chen, S. Zhao, A. Karnad, J. W. Freeman (2018) The biology and role of CD44 in cancer progression: therapeutic implications. *J. Hematol. Oncol.* **11**, 64.

36. L. T. Senbanjo, M. A. Chellaiah (2017) CD44: A Multifunctional Cell Surface Adhesion Receptor Is a Regulator of Progression and Metastasis of Cancer Cells. *Front. Cell Dev. Biol.* **5**, doi:10.3389/fcell.2017.00018.

37. P. M. Glumac, A. M. LeBeau (2018) The role of CD133 in cancer: a concise review. *Clin. Transl. Med.* **7**, doi:10.1186/s40169-018-0198-1.

38. J. Bie, X. Hu, M. Yang, X. Shi, X. Zhang, Z. Wang (2020) PTK7 promotes the malignant properties of cancer stem-like cells in esophageal squamous cell lines. *Hum. Cell*. **33**, 356–365.

39. S. J. A. Buczacki, S. Popova, E. Biggs, C. Koukorava, J. Buzzelli, L. Vermeulen,

L. Hazelwood, H. Francies, M. J. Garnett, D. J. Winton (2018) *J. Exp. Med.*, in press, doi:10.1084/jem.20171385.

40. G. Shi, O. Schwartz, A. A. Compton (2017), More than meets the I: the diverse antiviral and cellular functions of interferon-induced transmembrane proteins. *Retrovirology*. **14**, 53.

41. F. Yu, D. Xie, S. S. Ng, C. T. Lum, M.-Y. Cai, W. K. Cheung, H.-F. Kung, G. Lin, X. Wang, M. C. Lin (2015) IFITM1 promotes the metastasis of human colorectal cancer via CAV-1. *Cancer Lett.* **368**, 135–143.

42. A. Fatehullah, S. H. Tan, N. Barker (2016) Organoids as an in vitro model of human development and disease. *Nat. Cell Biol.* **18**, 246–54.

43. K. Kretzschmar, H. Clevers (2016) Organoids: Modeling Development and the Stem Cell Niche in a Dish. *Dev. Cell*. **38**, 590–600.

44. A. Merenda, A. Andersson-Rolf, R. C. Mustata, T. Li, H. Kim, B.-K. Koo (2017) A Protocol for Multiple Gene Knockout in Mouse Small Intestinal Organoids Using a CRISPR-concatemer A Protocol for Multiple Gene Knockout in Mouse Small Intestinal Organoids Using a CRISPR-concatemer. Video Link. *J. Vis. Exp*. **5591637915**, 1–8.

45. T. Matsui, T. Shinozawa (2021) Human Organoids for Predictive Toxicology Research and Drug Development. *Front. Genet.* **12**, doi:10.3389/fgene.2021.767621.

46. M. Van De Wetering, H. E. Francies, J. M. Francis, G. Bounova, F. Iorio, A. Pronk, W. Van Houdt, J. Van Gorp, A. Taylor-Weiner, L. Kester, A. McLaren-Douglas, J. Blokker, S. Jaksani, S. Bartfeld, R. Volckman, P. Van Sluis, V. S. W. Li, S. Seepo, C. Sekhar Pedamallu, K. Cibulskis, S. L. Carter, A. McKenna, M. S. Lawrence, L. Lichtenstein, C. Stewart, J. Koster, R. Versteeg, A. Van Oudenaarden, J. Saez-Rodriguez, R. G. J. Vries, G. Getz, L. Wessels, M. R. Stratton, U. McDermott, M. Meyerson, M. J. Garnett, H. Clevers (2015) Prospective derivation of a living organoid biobank of colorectal cancer patients. *Cell*. **161**, 933–945.

47. J. Drost, H. Clevers (2018) Organoids in cancer research. *Nat. Rev. Cancer*, 1.

48. Q. Ping, R. Yan, X. Cheng, W. Wang, Y. Zhong, Z. Hou, Y. Shi, C. Wang, R. Li (2021) Cancer-associated fibroblasts: overview, progress, challenges, and directions. *Cancer Gene Ther.* **28**, 984–999.

49. C. Strell, J. Paulsson, S.-B. Jin, N. P. Tobin, A. Mezheyeuski, P. Roswall, C. Mutgan, N. Mitsios, H. Johansson, S. M. Wickberg, J. Svedlund, M. Nilsson, P. Hall, J. Mulder, D. C. Radisky, K. Pietras, J. Bergh, U. Lendahl, F. Wärnberg, A. Östman (2019) Impact of Epithelial–Stromal Interactions on Peritumoral Fibroblasts in Ductal Carcinoma in Situ. *JNCI J. Natl. Cancer Inst.* **111**, 983–995.

50. E. Sahai, I. Astsaturov, E. Cukierman, D. G. DeNardo, M. Egeblad, R. M. Evans, D. Fearon, F. R. Greten, S. R. Hingorani, T. Hunter, R. O. Hynes, R. K. Jain, T. Janowitz, C. Jorgensen, A. C. Kimmelman, M. G. Kolonin, R. G. Maki, R. S. Powers, E. Puré, D. C. Ramirez, R. Scherz-Shouval, M. H. Sherman, S. Stewart, T. D. Tlsty, D. A. Tuveson, F. M. Watt, V. Weaver, A. T. Weeraratna, Z. Werb (2020) A framework for advancing our understanding of cancer-associated fibroblasts. *Nat. Rev. Cancer*. **20**, 174–186.

51. E. R. Abels, X. O. Breakefield (2016) Introduction to Extracellular Vesicles: Biogenesis, RNA Cargo Selection, Content, Release, and Uptake. *Cell. Mol. Neurobiol.* **36**, 301–312.

52. W. M. Henne, N. J. Buchkovich, S. D. Emr (2011) Review The ESCRT Pathway. *Dev. Cell*. **21**, 77–91.

53. J. Kowal, G. Arras, M. Colombo, M. Jouve, J. P. Morath, B. Primdal-Bengtson, F. Dingli, D. Loew, M. Tkach, C. Théry (2016) Proteomic comparison defines novel markers to characterize heterogeneous populations of extracellular vesicle subtypes. *Proc. Natl. Acad. Sci.* **113**, doi:10.1073/pnas.1521230113.

54. C. Théry, K. W. Witwer, E. Aikawa, M. J. Alcaraz, J. D. Anderson, R. Andriantsitohaina, A. Antoniou, T. Arab, F. Archer, G. K. Atkin-Smith, D. C. Ayre, J.-M. Bach, D. Bachurski, H. Baharvand, L. Balaj, S. Baldacchino, N. N. Bauer, A. A. Baxter, M. Bebawy, C. Beckham, A. Bedina Zavec, A. Benmoussa, A. C. Berardi, P. Bergese, E. Bielska, C. Blenkiron, S. Bobis-Wozowicz, E.

Boilard, W. Boireau, A. Bongiovanni, F. E. Borràs, S. Bosch, C. M. Boulanger, X. Breakefield, A. M. Breglio, M. Á. Brennan, D. R. Brigstock, A. Brisson, M. L. Broekman, J. F. Bromberg, P. Bryl-Górecka, S. Buch, A. H. Buck, D. Burger, S. Busatto, D. Buschmann, B. Bussolati, E. I. Buzás, J. B. Byrd, G. Camussi, D. R. Carter, S. Caruso, L. W. Chamley, Y.-T. Chang, C. Chen, S. Chen, L. Cheng, A. R. Chin, A. Clayton, S. P. Clerici, A. Cocks, E. Cocucci, R. J. Coffey, A. Cordeiro-da-Silva, Y. Couch, F. A. Coumans, B. Coyle, R. Crescitelli, M. F. Criado, C. D'Souza-Schorey, S. Das, A. Datta Chaudhuri, P. de Candia, E. F. De Santana, O. De Wever, H. A. del Portillo, T. Demaret, S. Deville, A. Devitt, B. Dhondt, D. Di Vizio, L. C. Dieterich, V. Dolo, A. P. Dominguez Rubio, M. Dominici, M. R. Dourado, T. A. Driedonks, F. V Duarte, H. M. Duncan, R. M. Eichenberger, K. Ekström, S. EL Andaloussi, C. Elie-Caille, U. Erdbrügger, J. M. Falcón-Pérez, F. Fatima, J. E. Fish, M. Flores-Bellver, A. Försönits, A. Frelet-Barrand, F. Fricke, G. Fuhrmann, S. Gabrielsson, A. Gámez-Valero, C. Gardiner, K. Gärtner, R. Gaudin, Y. S. Gho, B. Giebel, C. Gilbert, M. Gimona, I. Giusti, D. C. Goberdhan, A. Görgens, S. M. Gorski, D. W. Greening, J. C. Gross, A. Gualerzi, G. N. Gupta, D. Gustafson, A. Handberg, R. A. Haraszti, P. Harrison, H. Hegyesi, A. Hendrix, A. F. Hill, F. H. Hochberg, K. F. Hoffmann, B. Holder, H. Holthofer, B. Hosseinkhani, G. Hu, Y. Huang, V. Huber, S. Hunt, A. G.-E. Ibrahim, T. Ikezu, J. M. Inal, M. Isin, A. Ivanova, H. K. Jackson, S. Jacobsen, S. M. Jay, M. Jayachandran, G. Jenster, L. Jiang, S. M. Johnson, J. C. Jones, A. Jong, T. Jovanovic-Talisman, S. Jung, R. Kalluri, S. Kano, S. Kaur, Y. Kawamura, E. T. Keller, D. Khamari, E. Khomyakova, A. Khvorova, P. Kierulf, K. P. Kim, T. Kislinger, M. Klingeborn, D. J. Klinke, M. Kornek, M. M. Kosanović, Á. F. Kovács, E.-M. Krämer-Albers, S. Krasemann, M. Krause, I. V Kurochkin, G. D. Kusuma, S. Kuypers, S. Laitinen, S. M. Langevin, L. R. Languino, J. Lannigan, C. Lässer, L. C. Laurent, G. Lavieu, E. Lázaro-Ibáñez, S. Le Lay, M.-S. Lee, Y. X. F. Lee, D. S. Lemos, M. Lenassi, A. Leszczynska, I. T. Li, K. Liao, S. F. Libregts, E. Ligeti, R. Lim, S. K. Lim, A. Linē, K. Linnemannstöns, A. Llorente, C. A. Lombard, M. J. Lorenowicz, Á. M. Lörincz, J. Lötvall, J. Lovett, M. C. Lowry, X. Loyer, Q. Lu, B. Lukomska, T. R. Lunavat, S. L. Maas, H. Malhi, A. Marcilla, J. Mariani, J. Mariscal, E. S. Martens-Uzunova, L. Martin-Jaular, M. C. Martinez, V.

R. Martins, M. Mathieu, S. Mathivanan, M. Maugeri, L. K. McGinnis, M. J. McVey, D. G. Meckes, K. L. Meehan, I. Mertens, V. R. Minciacchi, A. Möller, M. Møller Jørgensen, A. Morales-Kastresana, J. Morhayim, F. Mullier, M. Muraca, L. Musante, V. Mussack, D. C. Muth, K. H. Myburgh, T. Najrana, M. Nawaz, I. Nazarenko, P. Nejsum, C. Neri, T. Neri, R. Nieuwland, L. Nimrichter, J. P. Nolan, E. N. Nolte-'t Hoen, N. Noren Hooten, L. O'Driscoll, T. O'Grady, A. O'Loghlen, T. Ochiya, M. Olivier, A. Ortiz, L. A. Ortiz, X. Osteikoetxea, O. Østergaard, M. Ostrowski, J. Park, D. M. Pegtel, H. Peinado, F. Perut, M. W. Pfaffl, D. G. Phinney, B. C. Pieters, R. C. Pink, D. S. Pisetsky, E. Pogge von Strandmann, I. Polakovicova, I. K. Poon, B. H. Powell, I. Prada, L. Pulliam, P. Quesenberry, A. Radeghieri, R. L. Raffai, S. Raimondo, J. Rak, M. I. Ramirez, G. Raposo, M. S. Rayyan, N. Regev-Rudzki, F. L. Ricklefs, P. D. Robbins, D. D. Roberts, S. C. Rodrigues, E. Rohde, S. Rome, K. M. Rouschop, A. Rughetti, A. E. Russell, P. Saá, S. Sahoo, E. Salas-Huenuleo, C. Sánchez, J. A. Saugstad, M. J. Saul, R. M. Schiffelers, R. Schneider, T. H. Schøyen, A. Scott, E. Shahaj, S. Sharma, O. Shatnyeva, F. Shekari, G. V. Shelke, A. K. Shetty, K. Shiba, P. R.-M. Siljander, A. M. Silva, A. Skowronek, O. L. Snyder, R. P. Soares, B. W. Sódar, C. Soekmadji, J. Sotillo, P. D. Stahl, W. Stoorvogel, S. L. Stott, E. F. Strasser, S. Swift, H. Tahara, M. Tewari, K. Timms, S. Tiwari, R. Tixeira, M. Tkach, W. S. Toh, R. Tomasini, A. C. Torrecilhas, J. P. Tosar, V. Toxavidis, L. Urbanelli, P. Vader, B. W. van Balkom, S. G. van der Grein, J. Van Deun, M. J. van Herwijnen, K. Van Keuren-Jensen, G. van Niel, M. E. van Royen, A. J. van Wijnen, M. H. Vasconcelos, I. J. Vechetti, T. D. Veit, L. J. Vella, É. Velot, F. J. Verweij, B. Vestad, J. L. Viñas, T. Visnovitz, K. V Vukman, J. Wahlgren, D. C. Watson, M. H. Wauben, A. Weaver, J. P. Webber, V. Weber, A. M. Wehman, D. J. Weiss, J. A. Welsh, S. Wendt, A. M. Wheelock, Z. Wiener, L. Witte, J. Wolfram, A. Xagorari, P. Xander, J. Xu, X. Yan, M. Yáñez-Mó, H. Yin, Y. Yuana, V. Zappulli, J. Zarubova, V. Žėkas, J. Zhang, Z. Zhao, L. Zheng, A. R. Zheutlin, A. M. Zickler, P. Zimmermann, A. M. Zivkovic, D. Zocco, E. K. Zuba-Surma (2018) Minimal information for studies of extracellular vesicles 2018 (MISEV2018): a position statement of the International Society for Extracellular Vesicles and update of the MISEV2014 guidelines. *J. Extracell. Vesicles*. **7**, 1535750.

55. E. I. Buzas, B. György, G. Nagy, A. Falus, S. Gay (2014) Emerging role of extracellular vesicles in inflammatory diseases. *Nat. Rev. Rheumatol.* **10**, 356–364.

56. B. György, T. G. Szabó, M. Pásztói, Z. Pál, P. Misják, B. Aradi, V. László, É. Pállinger, E. Pap, Á. Kittel, G. Nagy, A. Falus, E. I. Buzás (2011) Membrane vesicles, current state-of-the-art: emerging role of extracellular vesicles. *Cell. Mol. Life Sci.* **68**, 2667–2688.

57. M. Mathieu, L. Martin-Jaular, G. Lavieu, C. Théry (2019) Specificities of secretion and uptake of exosomes and other extracellular vesicles for cell-to-cell communication. *Nat. Cell Biol.* **21**, 9–17.

58. Z. Szvicsek, Á. Oszvald, L. Szabó, G. O. Sándor, A. Kelemen, A. Á. Soós, K. Pálóczi, L. Harsányi, T. Tölgyes, K. Dede, A. Bursics, E. I. Buzás, A. Zeöld, Z. Wiener (2019) Extracellular vesicle release from intestinal organoids is modulated by Apc mutation and other colorectal cancer progression factors. *Cell. Mol. Life Sci.* **76**, 2463–2476.

59. A. Zeöld, G. O. Sándor, A. Kiss, A. Á. Soós, T. Tölgyes, A. Bursics, Á. Szűcs, L. Harsányi, Á. Kittel, A. Gézsi, E. I. Buzás, Z. Wiener (2021) Shared extracellular vesicle miRNA profiles of matched ductal pancreatic adenocarcinoma organoids and blood plasma samples show the power of organoid technology. *Cell. Mol. Life Sci.* **78**, 3005–3020.

60. M. Berdiel-Acer, R. Sanz-Pamplona, A. Calon, D. Cuadras, A. Berenguer, X. Sanjuan, M. J. Paules, R. Salazar, V. Moreno, E. Batlle, A. Villanueva, D. G. Molleví (2014) Differences between CAFs and their paired NCF from adjacent colonic mucosa reveal functional heterogeneity of CAFs, providing prognostic information. *Mol. Oncol.* **8**, 1290–1305.

61. E. Elyada, A. Pribluda, R. E. Goldstein, Y. Morgenstern, G. Brachya, G. Cojocaru, I. Snir-Alkalay, I. Burstain, R. Haffner-Krausz, S. Jung, Z. Wiener, K. Alitalo, M. Oren, E. Pikarsky, Y. Ben-Neriah (2011) CKIα ablation highlights a critical role for p53 in invasiveness control. *Nature.* **470**, 409–413.

62. T. V. Petrova, A. Nykänen, C. Norrmén, K. I. Ivanov, L. C. Andersson, C. Haglund, P. Puolakkainen, F. Wempe, H. von Melchner, G. Gradwohl, S.

Vanharanta, L. A. Aaltonen, J. Saharinen, M. Gentile, A. Clarke, J. Taipale, G. Oliver, K. Alitalo (2008) Transcription Factor PROX1 Induces Colon Cancer Progression by Promoting the Transition from Benign to Highly Dysplastic Phenotype. *Cancer Cell*. **13**, 407–419.

63. A. G. Schepers, H. J. Snippert, D. E. Stange, M. van den Born, J. H. van Es, M. van de Wetering, H. Clevers (2012) Lineage Tracing Reveals Lgr5+ Stem Cell Activity in Mouse Intestinal Adenomas. *Science (80-.).* **337**, 730–735.

64. S. Weston, S. Czieso, I. J. White, S. E. Smith, P. Kellam, M. Marsh (2014) A Membrane Topology Model for Human Interferon Inducible Transmembrane Protein 1. *PLoS One*. **9**, e104341.

65. S. E. Smith, D. C. Busse, S. Binter, S. Weston, C. Diaz Soria, B. M. Laksono, S. Clare, S. Van Nieuwkoop, B. G. Van den Hoogen, M. Clement, M. Marsden, I. R. Humphreys, M. Marsh, R. L. de Swart, R. S. Wash, J. S. Tregoning, P. Kellam (2019) Interferon-Induced Transmembrane Protein 1 Restricts Replication of Viruses That Enter Cells via the Plasma Membrane. *J. Virol.* **93**, doi:10.1128/JVI.02003-18.

66. C. C. Bailey, G. Zhong, I.-C. Huang, M. Farzan (2014) IFITM-Family Proteins: The Cell's First Line of Antiviral Defense. *Annu. Rev. Virol.* **1**, 261–283.

67. S. Smith, S. Weston, P. Kellam, M. Marsh (2014) IFITM proteins—cellular inhibitors of viral entry. *Curr. Opin. Virol.* **4**, 71–77.

68. Á. Oszvald, Z. Szvicsek, M. Pápai, A. Kelemen, Z. Varga, T. Tölgyes, K. Dede, A. Bursics, E. I. Buzás, Z. Wiener (2020) Fibroblast-Derived Extracellular Vesicles Induce Colorectal Cancer Progression by Transmitting Amphiregulin. *Front. Cell Dev. Biol.* **8**, doi:10.3389/fcell.2020.00558.

69. R. A. Haraszti, M.-C. Didiot, E. Sapp, J. Leszyk, S. A. Shaffer, H. E. Rockwell, F. Gao, N. R. Narain, M. DiFiglia, M. A. Kiebish, N. Aronin, A. Khvorova (2016) High-resolution proteomic and lipidomic analysis of exosomes and microvesicles from different cell sources. *J. Extracell. Vesicles*. **5**, 32570.

70. F. Bray, J. Ferlay, I. Soerjomataram, R. L. Siegel, L. A. Torre, A. Jemal (2018)

Global cancer statistics 2018: GLOBOCAN estimates of incidence and mortality worldwide for 36 cancers in 185 countries. *CA. Cancer J. Clin.* **68**, 394–424.

71. D. Hanahan, R. A. Weinberg (2011) Hallmarks of cancer: The next generation. *Cell*. **144**, 646–674.

72. M. Ha, V. N. Kim (2014) Regulation of microRNA biogenesis. *Nat. Rev. Mol. Cell Biol.* **15**, 509–524.

73. J. P. Broughton, M. T. Lovci, J. L. Huang, G. W. Yeo, A. E. Pasquinelli (2016) Pairing beyond the Seed Supports MicroRNA Targeting Specificity. *Mol. Cell*. **64**, 320–333.

74. J. O'Brien, H. Hayder, Y. Zayed, C. Peng (2018) Overview of MicroRNA Biogenesis, Mechanisms of Actions, and Circulation. *Front. Endocrinol. (Lausanne).* **9**, doi:10.3389/fendo.2018.00402.

75. R. Bhome, F. Del Vecchio, G.-H. Lee, M. D. Bullock, J. N. Primrose, A. E. Sayan, A. H. Mirnezami (2018) Exosomal microRNAs (exomiRs): Small molecules with a big role in cancer. *Cancer Lett.* **420**, 228–235.

76. J. V Carter, N. J. Galbraith, D. Yang, J. F. Burton, S. P. Walker, S. Galandiuk (2017) Blood-based microRNAs as biomarkers for the diagnosis of colorectal cancer: a systematic review and meta-analysis. *Br. J. Cancer*. **116**, 762–774.

77. Z. Huang, S. Huang, Q. Wang, L. Liang, S. Ni, L. Wang, W. Sheng, X. He, X. Du (2011) MicroRNA-95 Promotes Cell Proliferation and Targets Sorting Nexin 1 in Human Colorectal Carcinoma. *Cancer Res.* **71**, 2582–2589.

78. Y. Lu, X. Zhao, Q. Liu, C. Li, R. Graves-Deal, Z. Cao, B. Singh, J. L. Franklin, J. Wang, H. Hu, T. Wei, M. Yang, T. J. Yeatman, E. Lee, K. Saito-Diaz, S. Hinger, J. G. Patton, C. H. Chung, S. Emmrich, J.-H. Klusmann, D. Fan, R. J. Coffey (2017) lncRNA MIR100HG-derived miR-100 and miR-125b mediate cetuximab resistance via Wnt/β-catenin signaling. *Nat. Med.* **23**, 1331–1341.

79. M.-K. Zhou, X.-J. Liu, Z.-G. Zhao, Y.-M. Cheng (2015) MicroRNA-100 functions as a tumor suppressor by inhibiting Lgr5 expression in colon cancer cells. *Mol. Med. Rep.* **11**, 2947–2952.

80. D. Chen, Y. Sun, Y. Yuan, Z. Han, P. Zhang, J. Zhang, M. J. You, J. Teruya-Feldstein, M. Wang, S. Gupta, M.-C. Hung, H. Liang, L. Ma (2014) miR-100 Induces Epithelial-Mesenchymal Transition but Suppresses Tumorigenesis, Migration and Invasion. *PLoS Genet.* **10**, e1004177.

81. J. Nie, L. Liu, W. Zheng, L. Chen, X. Wu, Y. Xu, X. Du, W. Han (2012) microRNA-365, down-regulated in colon cancer, inhibits cell cycle progression and promotes apoptosis of colon cancer cells by probably targeting Cyclin D1 and Bcl-2. *Carcinogenesis*. **33**, 220–225.

82. Y. Wang, S. Zhang, H. Bao, S. Mu, B. Zhang, H. Ma, S. Ma (2018) MicroRNA-365 promotes lung carcinogenesis by downregulating the USP33/SLIT2/ROBO1 signalling pathway. *Cancer Cell Int.* **18**, 64.

83. L. Zhou, Y. Wang, C. Ou, Z. Lin, J. Wang, H. Liu, M. Zhou, Z. Ding (2015) microRNA-365-targeted nuclear factor I/B transcriptionally represses cyclin-dependent kinase 6 and 4 to inhibit the progression of cutaneous squamous cell carcinoma. *Int. J. Biochem. Cell Biol.* **65**, 182–191.

84. M. Zhou, W. Liu, S. Ma, H. Cao, X. Peng, L. Guo, X. Zhou, L. Zheng, L. Guo, M. Wan, W. Shi, Y. He, C. Lu, L. Jiang, C. Ou, Y. Guo, Z. Ding (2013) A novel onco-miR-365 induces cutaneous squamous cell carcinoma. *Carcinogenesis*. **34**, 1653–1659.

85. J. Coon, K. Kingsley, K. M. Howard (2020) miR-365 (microRNA): Potential Biomarker in Oral Squamous Cell Carcinoma Exosomes and Extracellular Vesicles. *Int. J. Mol. Sci.* **21**, 5317.

86. Y. Sun, P. Sukumaran, A. Varma, S. Derry, A. E. Sahmoun, B. B. Singh (2014) Cholesterol-induced activation of TRPM7 regulates cell proliferation, migration, and viability of human prostate cells. *Biochim. Biophys. Acta - Mol. Cell Res.* **1843**, 1839–1850.

87. B. Huang, B. Song, C. Xu (2020) Cholesterol metabolism in cancer: mechanisms and therapeutic opportunities. *Nat. Metab.* **2**, 132–141.

88. M. E. Zettler, M. A. Prociuk, J. A. Austria, H. Massaeli, G. Zhong, G. N. Pierce

(2003) OxLDL stimulates cell proliferation through a general induction of cell cycle proteins. *Am. J. Physiol. Circ. Physiol.* **284**, H644–H653.

89. R. Liang, X. Li, X. Zhu (2020) Deciphering the Roles of IFITM1 in Tumors. *Mol. Diagn. Ther.* **24**, 433–441.

90. I. Novita Sari, Y.-G. Yang, L. T. Hanh Phi, H. Kim, M. Jun Baek, D. Jeong, H. Young Kwon, (2016) Interferon-induced transmembrane protein 1 (IFITM1) is required for the progression of colorectal cancer. *Oncotarget*. **7**, 86039–86050.

91. A. J. Lui, E. S. Geanes, J. Ogony, F. Behbod, J. Marquess, K. Valdez, W. Jewell, O. Tawfik, J. Lewis-Wambi (2017) IFITM1 suppression blocks proliferation and invasion of aromatase inhibitor-resistant breast cancer in vivo by JAK/STAT-mediated induction of p21. *Cancer Lett.* **399**, 29–43.

92. O. K. Provance, E. S. Geanes, A. J. Lui, A. Roy, S. M. Holloran, S. Gunewardena, C. R. Hagan, S. Weir, J. Lewis-Wambi (2021) Disrupting interferon-alpha and NF-kappaB crosstalk suppresses IFITM1 expression attenuating triple-negative breast cancer progression. *Cancer Lett.* **514**, 12–29.

93. H. Lickert, B. Cox, C. Wehrle, M. M. Taketo, R. Kemler, J. Rossant (2005) Dissecting Wnt/β-catenin signaling during gastrulation using RNA interference in mouse embryos. *Development*. **132**, 2599–2609.

94. P. Andreu, S. Colnot, C. Godard, P. Laurent-Puig, D. Lamarque, A. Kahn, C. Perret, B. Romagnolo (2006) Identification of the IFITM Family as a New Molecular Marker in Human Colorectal Tumors. *Cancer Res.* **66**, 1949–1955.

95. Y. Liao, M. U. Goraya, X. Yuan, B. Zhang, S.-H. Chiu, J.-L. Chen (2019) Functional Involvement of Interferon-Inducible Transmembrane Proteins in Antiviral Immunity. *Front. Microbiol.* **10**, doi:10.3389/fmicb.2019.01097.

96. A. R. Everitt, S. Clare, T. Pertel, S. P. John, R. S. Wash, S. E. Smith, C. R. Chin, E. M. Feeley, J. S. Sims, D. J. Adams, H. M. Wise, L. Kane, D. Goulding, P. Digard, V. Anttila, J. K. Baillie, T. S. Walsh, D. A. Hume, A. Palotie, Y. Xue, V. Colonna, C. Tyler-Smith, J. Dunning, S. B. Gordon, R. L. Smyth, P. J. Openshaw, G. Dougan, A. L. Brass, P. Kellam (2012) IFITM3 restricts the morbidity and

mortality associated with influenza. *Nature*. **484**, 519–523.

97. G. Savidis, J. M. Perreira, J. M. Portmann, P. Meraner, Z. Guo, S. Green, A. L. Brass (2016) The IFITMs Inhibit Zika Virus Replication. *Cell Rep.* **15**, 2323–2330.

98. K. Li, R. M. Markosyan, Y.-M. Zheng, O. Golfetto, B. Bungart, M. Li, S. Ding, Y. He, C. Liang, J. C. Lee, E. Gratton, F. S. Cohen, S.-L. Liu (2013) IFITM Proteins Restrict Viral Membrane Hemifusion. *PLoS Pathog.* **9**, e1003124.

99. N. M. Chesarino, A. A. Compton, T. M. McMichael, A. D. Kenney, L. Zhang, V. Soewarna, M. Davis, O. Schwartz, J. S. Yount (2017) IFITM3 requires an amphipathic helix for antiviral activity. *EMBO Rep.* **18**, 1740–1751.

100. E. Nolte-‘t Hoen, T. Cremer, R. C. Gallo, L. B. Margolis (2016) Extracellular vesicles and viruses: Are they close relatives? *Proc. Natl. Acad. Sci.* **113**, 9155–9161.

101. M. Mendt, S. Kamerkar, H. Sugimoto, K. M. McAndrews, C.-C. Wu, M. Gagea, S. Yang, E. V. R. Blanko, Q. Peng, X. Ma, J. R. Marszalek, A. Maitra, C. Yee, K. Rezvani, E. Shpall, V. S. LeBleu, R. Kalluri (2018) Generation and testing of clinical-grade exosomes for pancreatic cancer. *JCI Insight*. **3**, doi:10.1172/jci.insight.99263.

102. S. Kamerkar, V. S. LeBleu, H. Sugimoto, S. Yang, C. F. Ruivo, S. A. Melo, J. J. Lee, R. Kalluri (2017) Exosomes facilitate therapeutic targeting of oncogenic KRAS in pancreatic cancer. *Nature*. **546**, 498–503.

8. Bibliography of the candidate's publications

Publications used for the dissertation:

A. Kelemen, I. Carmi, Á. Oszvald, P. Lőrincz, G. Petővári, T. Tölgyes, K. Dede, A. Bursics, E. I. Buzás, Z. Wiener (2021) IFITM1 expression determines extracellular vesicle uptake in colorectal cancer. *Cell. Mol. Life Sci.* **78**, 7009–7024. **IF: 9.261**

A. Kelemen, I. Carmi, I. Seress, P. Lőrincz, T. Tölgyes, K. Dede, A. Bursics, E. I. Buzás, Z. Wiener (2022) CD44 Expression Intensity Marks Colorectal Cancer Cell Subpopulations with Different Extracellular Vesicle Release Capacity. *Int. J. Mol. Sci.* **23**, 2180. **IF: 5.924**

Other publications:

Á. Oszvald, Z. Szvicsek, M. Pápai, **A. Kelemen**, Z. Varga, T. Tölgyes, K. Dede, A. Bursics, E. I. Buzás, Z. Wiener (2020) Fibroblast-Derived Extracellular Vesicles Induce Colorectal Cancer Progression by Transmitting Amphiregulin. Front. Cell Dev. Biol. 8, doi:10.3389/fcell.2020.00558. **IF:6.684**

Á. Oszvald, Z. Szvicsek, G. O. Sándor, **A. Kelemen**, A. Á. Soós, K. Pálóczi, A. Bursics, K. Dede, T. Tölgyes, E. I. Buzás, A. Zeöld, Z. Wiener (2020) Extracellular vesicles transmit epithelial growth factor activity in the intestinal stem cell niche. Stem Cells. 38, 291–300. **IF:6.277**

Z. Szvicsek, Á. Oszvald, L. Szabó, G. O. Sándor, **A. Kelemen**, A. Á. Soós, K. Pálóczi, L. Harsányi, T. Tölgyes, K. Dede, A. Bursics, E. I. Buzás, A. Zeöld, Z. Wiener (2019) Extracellular vesicle release from intestinal organoids is modulated by Apc mutation and other colorectal cancer progression factors. Cell. Mol. Life Sci. 76, 2463–2476. **IF:6.496**

J. C. Sági, B. Egyed, **A. Kelemen**, N. Kutszegi, M. Hegyi, A. Gézsi, M. A. Herlitschke,

A. Rzepiel, L. E. Fodor, G. Ottóffy, G. T. Kovács, D. J. Erdélyi, C. Szalai, Á. F. Semsei (2018) Possible roles of genetic variations in chemotherapy related cardiotoxicity in pediatric acute lymphoblastic leukemia and osteosarcoma. BMC Cancer. 18, 704. **IF:2.933**

J. C. Sági, N. Kutszegi, **A. Kelemen**, L. E. Fodor, A. Gézsi, G. T. Kovács, D. J. Erdélyi, C. Szalai, Á. F. Semsei (2016) Pharmacogenetics of anthracyclines. Pharmacogenomics. 17, 1075–1087. **IF:2.35**

A. Rzepiel, N. Kutszegi, J. Cs. Sági, **A. Kelemen**, K. Pálóczi, Á. F. Semsei, E. Buzás, D. J. Erdélyi (2016) Extracelluláris vesiculák és hematológiai malignitásokban játszott szerepük. Orv. Hetil. 157, 1379–1384. **IF: 0.349**

DOI:10.14753/SE.2022.2728

9. Acknowledgments

I owe a debt of gratitude to Dr. Zoltán Wiener for being THE supervisor for me that every Ph.D. student only wishes for. During my Master's studies, he encouraged me not to finish my studies and continue with the Ph.D. program. He taught me all the basic and not basic molecular biology methods, critical thinking, and how to be and stay a motivated scientist even if the circumstances are not always the best. He answered all my questions every time and supported my aspirations. I am glad for the brainstorming that we had, I always felt I am a partner in these discussions and decisions and not just a subordinate who can only say yes to the orders. I am also thankful for the friendly, inspiring, and coffee-addicted atmosphere that he established in his lab.

I would like to thank Prof. Dr. Edit Buzás, Director of Semmelweis University, Department of Genetics, Cell- and Immunobiology for supporting my Ph.D. studies and providing a place for my research.

I am grateful for all the former and present members of the Molecular Cancer Biology Research Group. I thank Zsuzsanna Szvicsek that forming a friendly and supporting environment in the lab and also outside of it. I am thankful for all the coffees, the cookies, the supporting words, and the guidance in the EV isolation by the bead-based method. I thank Ádám Oszvald for all the funny moments and the guidance in RNA isolation, membrane labeling, and mouse experiments. I thank Dr. Anikó Zeöld for teaching me the tricks in ultracentrifugation and miRNA assay. I thank Gyöngyvér Orsolya Sándor for teaching me how to handle impossible situations. I thank András Áron Soós that I could count on him every time, we understood each other without words. It was a pleasure for being his colleague, I learned a lot about a good work attitude from him. As the phrase goes friendship has an end but lab partnership has no end and I hope once we can work together again. I thank Idan Carmi for improving my English language skills and having valuable research projects together. I also thank my interns, Idan Carmi and Iván Seress for teaching me how to guide students effectively. I am really proud of their successes at the Scientific Students' Associations Student Conference.

DOI:10.14753/SE.2022.2728

I am also grateful for the other members of the Department. I would like to highlight Anna Koncz who was always there for me if I needed any help. During our Ph.D. studies, we became real friends who can support each other mentally to not give up anything. I thank Alicia Galinsoga for having the opportunity to share my workaholism with someone in the lab, we were working next to each other at the late hours in the lab therefore I never felt alone.

I thank the Department for the enormous teaching opportunity, I became a better or at least more confident presenter by this.

I also thank all the co-authors of my articles for helping me reach my dream and the Richter Talentum Foundation for the scientifical and financial support. I especially thank Éva Andrásiné Antal for being supportive and answering all my questions related to my Richter Ph.D. Scholarship.

I am more than grateful to my best friend, Kinga Tóth, for always having a few good words and mexican food for me in every up and down. She always encouraged me not to give up and keep fighting.

I owe a debt of gratitude to my boyfriend, Dániel Bányay for helping in the bioinformatical analysis of my projects and being such a supportive partner during my Ph.D. studies as well. He was always holding my hand after every rejection and encouraged me not to give up. When I had to work at late hours or during the weekends he was understanding and pressed me to be a better scientist.

I thank my mother, Andrea Szlovák, and my grandmother Jolán Kara for supporting all of my moves and thoughts, and making it possible for me to be a Ph.D. student, and always believing in me.

And last but not least I would like to thank all the members of the doctoral committee for taking time with my dissertation and improving the scientific quality of it with their valuable advice.

DOI:10.14753/SE.2022.2728

10. Statement of originality

I, Andrea Kelemen (Neptun code: AVVRC5) hereby confirm that the content of this thesis is my own work. This thesis has not been submitted for any degree or other purposes. I certify that the intellectual content of this thesis is the product of my own work and that all the assistance received in preparing this thesis and sources have been acknowledged.

Budapest, 8th April, 2022

.....

Andrea Kelemen